國立臺灣大學獸醫專業學院分子暨比較病理生物學研究所

碩士論文

Graduate Institute of Molecular and Comparative Pathobiology
School of Veterinary Medicine
National Taiwan University

Master Thesis

新興小鼠毛蝨的外觀形態與分子特徵

Morphological and Molecular Characterization of a Novel Mouse Fur Mite

鄭穎謙

Ying-Chien Cheng

指導教授：萬灼華 博士

Advisor: Cho-Hua Wan, DVM, Ph.D.

中華民國 112 年 8 月

August, 2023

doi:10.6342/NTU202301649

致謝

在這四年就讀碩士學位的旅途中，一直以來都很感謝萬灼華老師教導我許多的專業知識、協助我研究論文撰寫與提點我做人處事的道理，讓我在這段過程中能夠得到許多的資源學習及成長進步，最後仍陪伴我完成這個學位並完整這個有深度的研究計畫，謝謝這段日子萬老師給予我許多的包容和支持鼓勵。在這個研究計畫中，特別感謝許多老師前輩們的指導:台大昆蟲系的柯俊成老師同意廖治榮學長指導我關於蟎類鑑定的各種技能與觀念，Georgia University 的 professor Anton 協助我們繪製很多 rRNA 二級結構圖，台大生化所的蕭超隆老師與欣怡助理學姐給予 RNA 萃取的技術與 rRNA secondary structure prediction 的觀念指導，台大食科所的謝淑貞老師讓我能順利操作 table-top SEM 及過去在實驗室的操作技術指導，還有中研院細生所的退休教授廖欽峯老師在論文撰寫上的建議和提醒，也很感謝台大外文系的 professor Vagios 在物種命名學上的分析與指導，讓我們能即時快速學習拉丁語系二名法命名的精髓，感謝緣分讓我能夠向各位老師前輩們學習。

在 LAM Lab 的這段日子，特別感謝星漙和 Celine 來到我們的研究室，在我後來的生活中給予我許多歡笑和陪伴，一同在實驗室中互相學習與協助，也互相支持鼓勵對方越來越進步與向前邁進，兩位學妹對我來說如同靈魂家人般的存在。也謝謝我的家人給我時間和支持，讓我能夠比較沒有後顧之憂去完成這個學位，同時體諒我也尊重我的學習步調。最後我也非常感謝我的男朋友冠宇，他在我這四年中也不厭其煩地陪伴我練習許多次的 seminar 或 conference 演講，他也知道 ribosomal RNA、Radfordia、Myocoptes、morphological and molecular characterization 等等非他專業的英文專有名詞或單字，也在這四年中給我很多鼓勵和支持，讓我能夠撐下去完成這個學業，是我很重要的人間淨土、避風港。

doi:10.6342/NTU202301649

這段日子其實有非常多想要感謝的人們，在這裡我統一感謝宇宙，謝謝宇宙的精心安排，讓我完整體驗這個研究過程的點點滴滴，讓我認識很多貴人和朋友們、學習很多新的知識事物、有機會去一趟美國參加研討會、在這個過程認識自己，讓我看見這個旅途中其實有很多的發光點，也看見自己後來的發光發熱，非常感謝宇宙帶給我這麼大的禮物和愛，謝謝祂帶給我這個漫長卻很值得的體驗，也謝謝自己的勇氣接受了這段旅途的過程，我辦到了！

穎謙　August 2023

doi:10.6342/NTU202301649

中文摘要

Myobia murismusculi (又名 *Myobia musculi*, MOB)、 *Radfordia affinis* (RDA)、*Myocoptes musculinus* (COP)是當代最常見的三種實驗小鼠外寄生蟲。臺灣大學獸醫專業學院實驗動物醫學診斷研究室例行性健康監測中，發現一個疑似新興毛蠕感染病例。在這個研究，我們根據外觀資料(結構與特徵)與分子生物數據(核醣體核醣核酸 ribosomal RNA [rRNA]與二級結構)以分析此新興毛蠕特徵與鑑定其物種分類，並將此小鼠毛蠕暫命名為 Species A (SPA)。我們將三種小鼠毛蠕 SPA、RDA 和 COP 的 18S 與 28S rRNA 的基因序列與其他過去已經發佈的蠕蟲基因做數據比較分析，18S 及 28S rRNA 基因的親緣分析顯示 SPA 與 MOB 及 RDA 應屬於同一個科(Myobiidae family)，而 COP 與 SPA 的親緣關係較遠。此外，28S rRNA 的二級結構比較顯示結構雖然相似，但部分區域的結構多樣性建議未來可應用於類似 SPA 新興毛蠕物種的分辨。在 SPA 與其他小鼠蠕蟲的外觀特徵比較顯示 SPA 與 MOB 在外觀上難以辨別，與 RDA 的體型大小相似，但微細結構特徵仍不同，而與 COP 外表形狀有明顯差異，因此根據外觀分析建議 SPA 是 *Myobia* 屬的新成員。這篇研究的結論支持 SPA 與 MOB 相近，且 SPA 是 Myobiidae 科 *Myobia* 屬的新發現小鼠毛蠕。

Keywords: 小鼠毛蠕、新興小鼠毛蠕、特徵化、外觀、分子生物

doi:10.6342/NTU202301649

Abstract

Myobia murismusculi (aka *Myobia musculi*, MOB), *Radfordia affinis* (RDA) and *Myocoptes musculinus* (COP) are the three most prevalent ectoparasite species in contemporary laboratory mice. In this study, based on the morphological and molecular evidences and the predicted secondary structures of ribosomal RNA (rRNA), we have identified and characterized a novel fur mite from naturally infested laboratory mice and designated as Species A (SPA). The nucleotide sequences of the 18S and/or 28S rRNA genes of SPA, RDA, and COP were determined and compared with other previously characterized mites. Phylogenetic analysis results of the 18S and/or 28S rRNA gene sequences revealed that SPA belongs to the same family as MOBs and RDAs, and COP is least related to SPA. Genetic distance results indicated that SPA is most closely related to MOBs and RDAs, but distinctly different from COP. The comparison of the predicted secondary structures of 28S rRNA revealed that structural variations could be possibly applied in differentiating SPA-like organisms from other fur mites in the future. Comparison of morphological characters of SPA and other mouse fur mites showed that SPA is externally indistinguishable from MOB, with similar shape/size but different external structures to RDA, and highly distinct to COP in shape and externals. SPA was a novel member of *Myobia* genus. In conclusion, SPA was a novel member of *Myobia* genus in the family Myobiidae with MOB.

Keywords: mouse fur mite, novel mouse fur mite, characterization, morphology, molecular biology

doi:10.6342/NTU202301649

Contents

doi:10.6342/NTU202301649

doi:10.6342/NTU202301649

List of Figures

Figure

doi:10.6342/NTU202301649

List of Tables

Table

doi:10.6342/NTU202301649

Introduction

More than 250 species of mites have been reported to cause health-related problems in domestic animals (Mullen *et al.*, 2019). *Myobia murismusculi* (aka *Myobia musculi,* MOB) and *Radfordia affinis* (RDA), and *Myocoptes musculinus* (COP) are the most common ectoparasites and can cause persistent infestations and management challenges in contemporary laboratory mouse colonies (National Research Council, 1991; Baker, 1998; Baker, 2007; Mullen *et al.*, 2019). These three mouse fur mites have been identified for at least 120 years, MOB (Schrank, 1781), RDA (Poppe, 1896), and COP (Koch, 1840) (Bochkov, 2009; Bochkov, 2010; Mullen *et al.*, 2019). In the past 50 years, fur mite-related research is mainly focused in the topics of animal diseases/research complication, treatment, diagnostic methods, infestation control/prevention, and prevalence/survey; limited research and/or new finding is emphasized in the field of entomology (Baker, 2007; Mullen *et al.*, 2019).

Myobia musculi (MOB) is a non-burrowing mouse fur mite in the genus *Myobia* of the family Myobiidae. The mite is very small, unsclerotized, elongate, with transverse integumental striae and bulges on the lateral margins between legs II-IV (National Research Council, 1991; Baker, 2007; Mullen *et al.*, 2019). The female and male are similar in external appearance, but vary in size, setation, and genitalia (Bochkov, 2009). The mite is about twice as long as it is wide, about 400–500 μm in length for females and about 280–300 μm in length for males. MOB has four pairs of legs, legs I-IV. Legs I are short, compressed, and adapted for hair clasping and each pair of legs II-IV has an empodial claw on each tarsus end. Both anus and genitalia are on the dorsum. The

doi:10.6342/NTU202301649

complete life cycle of MOB is approximately 23 days, including egg hatching stage (about 7 to 8 days), larva and nymph stages, and adult period (National Research Council, 1991; Baker, 2007; Mullen *et al.*, 2019). Within 24 hours, the adults are capable to lay oval-shaped eggs attaching to hairs near the base. Adults feed on skin secretions and interstitial fluid, but not on blood.

Radfordia affinis (RDA) is a non-burrowing mouse fur mite in the genus *Radfordia* of the family Myobiidae and morphologically very similar to MOB (National Research Council, 1991; Baker, 2007; Mullen *et al.*, 2019). Female and male mites are similar in elongated shape, but different in size, setation, and genitalia (Bochkov, 2009). RDA, also with lateral bulges between legs, is not easily differentiated from MOB by externals (size, shape, gnathosoma, legs, and genitalia/anus). RDA is differentiated from MOB by examining the ends of tarsus of the legs II, RDA with two tarsal claws and MOB with an empodial claw. The RDA life cycle has not been well studied and is assumed to be biologically similar to that of MOB (Baker, 2007; Mullen *et al.*, 2019). Adults feed on skin secretions and interstitial fluid, but not on blood.

Myocoptes musculinus (COP) is a non-burrowing mite in genus *Myocoptes* of the family Myocoptidae. Externally, COP is easily differentiated from MOB and RDA and the appearance of female and male mites is distinctly different in shape, size, and external fine structures (National Research Council, 1991; Baker, 2007; Bochkov, 2010; Mullen *et al.*, 2019). The female is white, oval-shaped (300–380 μm × 130 μm), with minute denticle-like striae on ventral idiosoma and scale-like ones on dorsum. COP has four pairs of legs (legs I-IV) with six free segments, legs I & II terminating in short stalks and ambulacral suckers and dark brown legs III & IV with enlarged and strongly

doi:10.6342/NTU202301649

chitinized modification for hair clasping. The chelicerae are large and chelate. Distinct from MOB and RDA, both genital opening and anus are on the ventral side, genital opening between legs IV and anus at posterior end. The male is smaller (about 160–210 μm × 135 μm) and less striated than the female. The male is similar to the female for the body portion anterior to legs III, but the posterior portion is different, including morphology of legs IV and posteriorly bilobate idiosoma. Greatly enlarged legs IV, with five free segments, are oriented posteriorly and used for grasping the female during copulation, not for clasping the hairs. Both anus with a small pair of suckers and a deltoid genital opening with the aedeagus are located on the ventral side. A complete life cycle of COP, including egg hatching (about 5 days), larva and nymph stages, and adult period is about 14 days (Baker, 2007; Mullen *et al.*, 2019). Unlike to MOB and RDA, COP eggs are usually attached to the distal end of hairs. COP mainly feeds on superficial epidermal layers, but not on blood (Baker, 2007).

Transmission of these fur mites from infested mice to naive mice require close and direct contact, not effective through contaminated bedding (Thigpen *et al.*, 1989; Baker, 2007; Lindstrom *et al.*, 2011). During infestation, MOB and RDA commonly occupy areas of the face, head, neck, shoulders, and flank, and COP tends to spread out over larger areas, including the inguinal areas, ventral side, back, base of the tail, and even to face/head/neck area (Baker, 2007). These three mouse fur mites usually cause subclinical infestation in laboratory mice. However, in severe infestation or susceptible sensitive strains (C57BL/6, NC/Jic, NC/Kuj, or BALB/c), mild alopecia, erythema, pruritus, traumatic dermatitis, ulceration/pyoderma, and/or decreases in body weight/life span/reproductive indices (Morita *et al.*, 1999; Baker, 2007; Johnston *et al.*, 2009). In addition, more reported research complications include lymphadenopathy,

doi:10.6342/NTU202301649

lymphocytopenia, granulocytosis, and extensive mast cell infiltration in cutaneous lesions and lymphoid tissues, hypergammaglobulinemia, affected IgE/IgG/IgM responses and ILs production (Morita *et al.*, 1999; Pochanke *et al.*, 2006; Baker, 2007; Johnston *et al.*, 2009).

Traditional methods applied in fur mite diagnosis, mainly based on the observation and distinct morphology of different mites include tape test, pluck test, and pelt examination. For the tape test and pluck test (antemortem methods), the microscopic examination of the tape-impressed samples and fur pluck samples collected from specific fur areas has been applied in detecting fur mites (Baker, 2007). The pelt exam (postmortem method), the traditional "gold standard" method for fur mite diagnosis is to directly screen the specific area of pelt from dead mice for the existence of eggs and mites under dissecting microscope (Baker, 2007; Karlsson *et al.*, 2014). However, these traditional diagnosis methods are less sensitive because of light infestation, species with similar external morphology (MOB/RDA), improper sampling sites, and personnel skills. Recently, PCR has been applied as a modern method to diagnose the infestation of mouse fur mites sensitively and specifically (Weiss *et al.*, 2012; Karlsson *et al.*, 2014; Gerwin *et al.*, 2017; Lee *et al.*, 2019; Chou *et al.*, 2020). Furthermore, without animal suffering and sacrifice, multiple PCR samples, including fur swab, cage wipe, individually ventilated cages (IVC) environmental wipe, and feces have been reported to be effective in evaluating the contamination status of fur mites in mouse colonies (Weiss *et al.*, 2012; Karlsson *et al.*, 2014; Gerwin *et al.*, 2017; Lee *et al.*, 2019; Chou *et al.*, 2020).

There were two fur mite monitoring cases with inconsistent results of pelt

doi:10.6342/NTU202301649

examination and PCR testing (Unpublished data, NTU Laboratory Animal Medicine Diagnostic Laboratory). The identification and molecular and morphological characterization of a novel mouse fur mite have been performed and all data suggest that this novel fur mite is a new member of *Myobia* genus in the family Myobiidae with MOB and RDA. In this study, the novel mouse fur mite was designated Species A (SPA).

doi:10.6342/NTU202301649

Methods and materials

Animal and fur mite samples

All animals were handled according to protocols approved by the Institutional Animal Care and Use Committee in National Taiwan University and the procedures were complied with the Animal Protection Act (2021) and Guideline for the Care and Use of Laboratory Animals in Taiwan (2018). A total of 32 mice were collected from two research facilities with fur mite infestation history, including nine ICR mice, 10 ICR genetically-engineered mice (GEM), 12 B6CBA GEM and one B6.129S6 GEM (Table 1). These mice varied in age, including two young adults (4 weeks $\leqq$ age $\leqq$ 8 weeks), one middle-aged mouse (8 weeks $\leqq$ age $\leqq$ 16 weeks), and 29 mice older than 16 weeks. Pelage was collected and examined under a dissecting microscope (Nikon SMZ800, Melville, New York, USA) for the presence of fur mites after CO_2 euthanasia. Fur mites (Table 2) were individually collected and stored at -80 °C for future use.

DNA extraction

Total DNA was extracted from individual fur mites which were digested for 14 to 18 h in ATL buffer by using the QIAamp® DNA Mini Kit (Qiagen, Hilden, Germany), according to the manufacturer's instructions, with some modifications suggested by Grove *et al.* (2012) and Chou *et al.* (2020). After total DNA extraction, fur mite shells were collected for further slide specimen preparation and morphological examination. Extracted DNA samples were stored at -20 °C until use.

Oligonucleotide primers

doi:10.6342/NTU202301649

Oligonucleotide primers were selected based on alignments performed with MegAlign software (DNASTAR, Madison, Wisconsin, USA). Primers were initially designed from the 18S rRNA and 28S rRNA gene sequences that are highly conserved among *Radfordia affinis, Myobia musculi, Myocoptes musculinus, Demodex brevis, Demodex folliculorum,* and *Crocidurobia* sp. The primers, targeting the 18S rRNA genes of mouse fur mites and the 28S rRNA genes of mites were also applied in this study (Chou *et al.*, 2020 and Zhao *et al.*, 2020). As sequence data of the 18S rRNA and 28S rRNA genes of fur mites became available, these data were applied in the design of additional primers. The oligonucleotide primers were synthesized by Invitrogen Life Technologies (Thermo Fisher Scientific, Waltham, Massachusetts, USA) or the Center of Biotechnology, National Taiwan University (NTU, Taipei, Taiwan, ROC).

DNA amplification

DNA amplification was performed in a 50 μL volume in an automated thermocycler (LabCycler 96, Sensoquest, Gottingen, Germany). Each PCR mixture contained 5 μL of DNA sample, 0.5 μM of each oligonucleotide primer, 0.2 mM of each dNTP (Promega, Madison, WI, USA), 1× Green GoTaq® Flexi Buffer (Promega), 1.5–2.0 mM $MgCl_2$ (Promega) and 1.25 U of GoTaq® Flexi DNA Polymerase (Promega). PCR consisted of 120 s denaturation at 95 °C, followed by 40 cycles of 95 °C for 30 s, 48–59 °C for 30 s and 72 °C for 30–60 s, and then 4 ˚C thereafter. Annealing temperature and length of elongation time varied depending on the primers used and the sizes of expected amplified products. The PCR-amplified products (10 μL) were electrophoresed in 2% agarose gels, stained with ethidium bromide, and visualized by UV light.

doi:10.6342/NTU202301649

DNA sequencing analysis and secondary structure prediction of 18S rRNA/28S rRNA gene

The PCR-amplified DNA fragments were purified by the QIAquick® PCR Purification Kit (Qiagen) or the QIAquick® Gel Extraction Kit (Qiagen) using protocols recommended by the manufacturer. DNA sequences were determined by the Sanger dideoxy-chain termination method with the BigDye Terminator v3.1 Cycle Sequencing Kit in the Center of Biotechnology, NTU. Sequence data were analyzed with EditSeq™ and MegAlign™ software of Lasergene® (DNASTAR) and MEGA X software (Kumar *et al.*, 2018). Phylogenetic analysis was performed by IQ-tree program (Trifinopoulos *et al.*, 2016) and then modified by FigTree v1.4.4 software (http://tree.bio.ed.ac.uk/software/figtree/ in https://beast.community/figtree) (BEAST developers, the University of Auckland, New Zealand). The sequences used for comparison were published sequences of mites of animals or plants which belong to related taxa (Table 3), animal mites including *Radfordia affinis* (MN153812), *Myobia musculi* (JF934703 and JF834895) (Feldman *et al.*, 2011), *Radfordia ensifera* (MN514776), *Radfordia elegantula* (KY922178) (Klimov *et al.*, 2017), *Radfordia lemnina* (KY922180) (Klimov *et al.*, 2017), *Caenolestomyobia faini* (KY922177) (Klimov *et al.*, 2017), and *Crocidurobia* sp. (KY922179 and KY922050) (Klimov *et al.*, 2017) in superfamily Myobioidea, *Demodex brevis* (GU377178 and HQ718592) (Zhao *et al.*, 2012) and *Demodex folliculorum* (GU377177 and HQ728000) (Zhao *et al.*, 2012) in superfamily Cheyletoidea, and *Myocoptes musculinus* (KT384411 and KT384412) (Lee *et al.*, 2019) in superfamily Sarcoptoidea; plant mites including *Favognathus* sp. (KY922193 and KY922064) (Klimov *et al.*, 2017) and *Raphignathus* sp. (KY922192 and KY922063) (Klimov *et al.*, 2017) in superfamily Raphignathoidea, *Linotetranidae*

doi:10.6342/NTU202301649

gen. sp. (KY922194 and KY922065) (Klimov *et al.*, 2017), *Tenuipalpus* sp. (KY922198 and KY922069) (Klimov *et al.*, 2017), *Tetranychus urticae* (AB926312 and KY922068) (Klimov *et al.*, 2017), and *Eotetranychus* sp. (KY922195 and KY922066) (Klimov *et al.*, 2017) in superfamily Tetranychoidea.

The predictions of the secondary structures of the present study 18S and the 28S rRNA began with the *Drosophila melanogaster* 18S and 28S rRNA as the template, obtained from the RiboVision 2.0 server (http://apollo.chemistry.gatech.edu/RiboVision2) (Bernier *et al.*, 2014). The predicted secondary structures of 18S rRNA (SPA, RDA-NTU, COP-NTU, and MOB) and 28S rRNA (SPA, RDA-NTU, and COP) were edited and modified with the program XRNA-GT (https://github.com/LDWLab/XRNA-GT). The predicted secondary structures were presented with domains, including the four domains (5', central, 3'-major, and 3'-minor) in the 18S rRNA and the six domains (I-VI) in the 28S rRNA.

Morphological examination of fur mites

Mite specimens were individually mounted in Hoyer's medium and examined under an optical microscope (Olympus BX51, Olympus Corp., Tokyo, Japan) for photo and drawing data. Measurements were taken by using stage-calibrated ocular micrometers and ImageJ 1.47 (Schneider *et al.*, 2012). All measurements were provided in micrometers (μm). Holotype measurements are shown in bold type for new species, followed by their average and range in parenthesis. Tabletop scanning electron microscope (TSEM) observations were performed using an TM3000 tabletop scanning electron microscope (Hitachi High-Technologies Corp., Tokyo, Japan). The mite specimens were placed on flat specimen holders with carbon conductive tape, avoid to mites being blown away in vacuum environment. All mite specimens were deposited in

doi:10.6342/NTU202301649

the Department of Veterinary Medicine, NTU.

doi:10.6342/NTU202301649

Results

Identification of non-MOB/RDA/COP fur mites in mice

A total of 32 laboratory mice were obtained from two different research colonies with fur mite infestation history (Colonies A, B). No clinical signs or external abnormalities were observed. The pelts of these mice were found to be positive on fur mite infestation under ectoparasite examination (Table 1). In Colony A, nineteen mice were diagnosed with mixed infestation of three different fur mites, externally consisting with MOB, RDA, and COP. In Colony B, two different fur mites, externally consisting with MOB and COP were detected on every mouse. To confirm the results of ectoparasite examination, the MOB/RDA-specific PCR and COP-specific PCR assays (Chou *et al.*, 2020) were applied to check the samples from these 32 mice (Fig 2). Based on results of the specific PCR tests, Colony A was positive on MOB/RDA (19/19) (Fig 2A) and COP (19/19) (Fig 2B), consisting with the results of pelt examination. And, the specific PCR results revealed that mice from Colony B were positive only on COP (13/13) (Fig 2B), but negative on MOB/RDA (0/13) (Fig 2A), indicating that these 13 mice in Colony B were free of MOB and RDA. For Colony B, the MOB/RDA-specific PCR result was inconsistent with the pelt exam result. In addition, the fur mite generic PCR testing followed by DNA sequencing was applied to evaluate these 32 samples from these two colonies. Results of the generic PCR and DNA sequencing revealed that both RDA and COP were detected in all mice (19/19) from Colony A and only COP was detected in Colony B mice (13/13). Furthermore, sequences of unknown mites, highly conserved but different from the DNA sequences of MOB, RDA, COP, and other published fur mites, were detected in all mice from both Colony A (19/19) and Colony B (13/13). The novel fur mites, non-MOB/RDA/COP, infesting mice in both colonies

doi:10.6342/NTU202301649

were further molecularly and morphologically characterized.

DNA sequence analysis

Genomic sequences of the non-MOB/RDA/COP mites corresponding to the 18S rRNA gene (nucleotides 1–1715; KT384411) and the 28S rRNA gene (nucleotides 37–3658; KT384412) of COP were determined from individual mites collected from infested mice of two colonies (Table 2). Additionally, the 18S and the 28S rRNA gene sequences of RDA (RDA-NTU) and COP (COP-NTU) identified in these two colonies were also determined (Table 2). The non-MOB/RDA/COP mites from these two colonies were found to be 99.8–100% identical in the 18S and 28S rRNA gene sequences, respectively. Therefore, the non-MOB/RDA/COP mites collected from two different colonies were the same species and designated species A (SPA). Comparison of the 18S rRNA gene sequence alignment of the newly identified SPA with RDA-NTU, COP-NTU and other previously reported mites of animals and plants revealed that SPA was most closely related to several rodent fur mites in superfamily Myobioidea (96.1–98.8% identity) (Table 4A), especially MOBs and RDAs (~ 98.8% identity). Mites in other superfamilies including Raphignathoidea, Tetranychoidea and Cheyletoidea showed 88.0–91.5% nucleotide identity with SPA. Another mouse fur mite, COPs in superfamily Sarcoptoidea were most distinct to SPA (86.5% nucleotide identity). RDA-NTU and COP-NTU were almost identical (99.7% and 99.9%) to previously published RDA and COP, respectively.

Comparison of the 28S rRNA gene sequence alignment of SPA with RDA-NTU and other mites of animals and plants revealed that SPA was most closely related to RDA-NTU (93.6% identity) (Table 4B). Both SPA and RDA-NTU were also close to *Crocidurobia* sp., a rodent fur mite in superfamily Myobioidea (87.8% and 89.4%

doi:10.6342/NTU202301649

identity, respectively). SPA and RDA-NTU were distinct to several plant mites in superfamilies Raphignathoidea and Tetranychoidea (72.5–78.7% nucleotide identity), the *Demodex* mites (71.2–75.0% nucleotide identity) in superfamily Cheyletoidea and COP (74.7% identity) in superfamily Sarcoptoidea.

The phylogenetic relationships of SPA, RDA-NTU, COP-NTU, and other previously published mites were constructed using the 18S rRNA (Fig 3A) and 28S rRNA gene sequences (Fig 3B). The phylogeny of the 18S rRNA analysis revealed that SPA was different, but most close to the subgroup of the RDA-NTU, MOBs, RDA, and *Radfordia elegantula* (KY922178), and also close to other rodent mites in Myobioidea superfamily. RDA-NTU was highly related to MOBs and RDA. The phylogeny analysis revealed that COP-NTU and the previously identified COP were extremely close to each other and should be recognized as the same organism in Sarcoptoidea superfamily. The phylogeny of the 28S rRNA analysis revealed that high divergency among different mite species was noticed. SPA and RDA-NTU were most closely related to each other, also close to the other rodent fur mite (*Crocidurobia* sp.) in the superfamily Myobioidea, and distinct to mites in other superfamilies (Raphignathoidea, Tetranychoidea and Cheyletoidea).

Ribosomal RNA secondary structure prediction

The secondary structures of the 18S rRNA (SPA, MOB, RDA-NTU, COP-NTU) (Fig 4A) and the 28S rRNA (SPA, RDA-NTU, and COP) (Fig 4B) were predicted. The structural domains in 18S rRNA (5’, central, 3’-major, and 3’-minor domains) and 28S rRNA (I-VI domains) were illustrated in different colors. Among these mite species, the common core of the 18S and the 28S rRNAs were conserved in the secondary structures. The variations are primarily noticed on the surface regions and the sizes of the

doi:10.6342/NTU202301649

ribosomes are different. For the 18S rRNAs, the secondary structures of the four mites are nearly identical, with minor differences in the 5’ domain (COP-NTU vs. SPA/MOB/RDA-NTU). For the 28S rRNAs, structural variations are noticed in three fur mite species (SPA, RDA-NTU, and COP), particularly the rRNA fragments in domains II, III and VI (Fig 4B). Among these, the 28S rRNA fragment variants have different secondary structures and lengths.

The morphology of SPA, RDA-NTU, and COP-NTU

Adult fur mites, including 118 SPAs (85 females and 33 males), 63 RDA-NTUs (49 females and 14 males), and 77 COP-NTUs (49 females and 28 males) were collected after pelt examination (Table 2). External morphology characters of 92 SPA, 55 RDA-NTU, and 33 COP-NTU were examined and recorded (photo, drawing, and/or size measure) under a light microscope (Fig 5) and hand drawing (Fig 6-10). Twenty-six SPAs, 8 RDA-NTUs, and 44 COP-NTU were examined under a tabletop scanning electron microscope (TSEM) (Fig 11) (Table 2).

SPA

Female and male mites exhibited similar body shapes, being small and elongate. The body length was approximately twice longer than width, approximately 484 (315–559) μm long in females and 346 (282–393) μm long in males. Both female and male possessed comparable main body structures, including gnathosoma (Fig 6A), four pairs of legs, and posterior body (idiosoma). The gnathosoma was smaller and shorter than the first pair of legs (legs I), featuring minute palpi and stylet-like chelicerae (Fig 11). Legs I were short/compressed in shape, well-adapted for hair clasping. Each tarsus end in the legs II-IV exhibited a noticeable character, empodial claw, which was a large

doi:10.6342/NTU202301649

single claw. Bulges were observed between each pair of legs II-IV on the lateral margins of idiosoma. The transverse integumental striae were prominently visible on the idiosoma surface under a TSEM (Fig 11A & 11B). In addition, a series of large, slightly expanded, fluted setae were observed on the dorsum, with distinct difference in location, size, and numbers between sexes (Fig 7 & 8). The genitalia were located on the dorsal surface (Fig 7 & 8), with an elongate and internal penis (aedeagus) positioned in middle for males, and a posterior opening for females. The anus was located at posterior end for both males and females.

RDA-NTU

Morphologically, RDA-NTU exhibited consistency with the external characters of RDA previously described (Baker, 2007; Bochkov, 2009) and also similarity to the newly-identified SPA (Fig 5A & 5B). Both female and male mites displayed an elongated shape, approximately 485 (396–541) μm long in females and 326 (222–389) μm long in males. The structures of gnathosoma, legs, and genitalia/anus closely resembled those of SPA (Fig 6A), with the exception of two tarsal claws on legs II in RDA-NTU. The location, size, and numbers of setae on RDA-NTU, with variation for different the sex, were consistent with those observed in RDA (Bochkov, 2009) (Fig 9).

COP-NTU

The morphology of COP-NTU exhibited consistency with the external structures of COP previously published (Baker, 2007; Bochkov, 2010). There were distinct differences in shape, size and external fine structures between both sexes (Fig 5C). Female displayed an oval shape, approximately 496 (448–544) μm long and 256 (233–278) μm wide. The gnathosoma had large and chelate chelicerae (Fig 6B). For

doi:10.6342/NTU202301649

idiosoma, the dorsum had scale-like striae, while the ventral side had with minute denticles (Fig 11E). Legs I and II consisted of six free segments and terminating in short stalks with ambulacral suckers. Legs III and IV were enlarged and strongly sclerotized, consisting of six segments without ambulacral suckers. The location, size, and numbers of setae on COP-NTU were consistent to those observed in female COP (Bochkov, 2010) (Fig 10A & 10B). On the ventral side, the genitalia opening was situated between the fourth pair of legs, and the anus was at posterior end. In comparison, the male was smaller, 328 (316–338) μm long and 218 (187–238) μm wide. They exhibited fewer striae on dorsum, and lacked denticles on the ventral side. The anterior portion of the male, anterior to the third pair of legs, resembled that of the female, but the posterior portion was distinctly different. The fourth pair of legs in male was greatly enlarged and consisted of five segments. The location, size, and numbers of setae on COP-NTU were consistent to those on male COP (Bochkov, 2010) (Fig 10C & 10D). On the ventral side, the aedeagus was located in a deltoid genital opening between the fourth pair of legs and the anus was accompanied by a small pair of suckers at posterior end. The idiosoma exhibited a posteriorly bilobated structure in the middle of genitalia opening and anus (Fig 11F).

The body size, numbers, location, and length of setae on idiosoma and each leg, the number of claws on each leg, and the setae of genitalia were focused and recorded for external characterization (Appendices 1–3).

doi:10.6342/NTU202301649

Discussion

Myobia musculi (MOB), *Radfordia affinis* (RDA), and *Myocoptes musculinus* (COP) are among the most common ectoparasites and cause a challenging problem in contemporary laboratory mouse colonies (National Research Council, 1991; Baker, 1998; Baker, 2007; Gerwin *et al.*, 2017; Körner, 2019). Recently, to improve the sensitivity of traditional diagnostic methods, molecular diagnostics has been developed and applied in parasite infestation monitoring for laboratory mice (Gerwin *et al.*, 2017; Lee *et al.*, 2019; Chou *et al.*, 2020). In this study, a new mouse fur mite, with MOB-like morphology but different genetic sequences, was identified from infested laboratory mice. This novel mouse fur mite Species A (SPA), characterized molecularly (18S and 28S rRNA genes) and morphologically, was classified as a member in *Myobia* genus of Myobiidae family.

Many novel pathogens have been discovered in laboratory rodents since 1990s, through clinical and/or histopathologic diseases, cell contamination, aberrant results of improved diagnostic assays (serology or molecular biology) (Ball-Goodrich *et al.*, 1994; Wan *et al.*, 2002; Wobus *et al.*, 2004; Roediger *et al.*, 2018). In many diagnostic laboratories, a molecular PCR assay has been developed and replaced the traditional pelt examination to improve the sensitivity and animal welfare for mouse fur mite monitoring (Gerwin *et al.*, 2017; Körner *et al.*, 2019; Lee *et al.*, 2019; Chou *et al.*, 2020; Hanson *et al.*, 2021). Through the improvement of fur mite assay in NTU Laboratory Animal Medicine Diagnostic Laboratory, the mouse fur mite PCR testing only detected COP, but not MOB in the colony B, with an endemic history of MOB and COP infestation according to previous health monitoring results. This unexpected diagnostic data initiates this study to identify and characterize this “MOB-like” novel mouse fur

doi:10.6342/NTU202301649

mite Species A.

To distinguish different mite species, either molecular or morphological analyses have been applied (Feldman *et al.*, 2011; Zhao *et al.*, 2013; Morita *et al.*, 2018; Liao *et al.*, 2021); however, limited studies have applied both systems to characterize a novel species at the same time (Matsuda *et al.*, 2013). In this study, the novel fur mite SPA was classified based on molecular and morphological data simultaneously. In entomology, the traditional and standard system to classify an arthropod is by external morphology, including detailed information of body size, shape, and fine structures (length, location, and numbers of setae and claw) (Docampo, 2017). Morphological characters of SPA are externally indistinguishable from those of MOB (Baker, 2007; Bochkov, 2009), with similar shape/size but different external fine structures to RDA, and highly distinct to COP in shape and externals (Figs 5-11, Appendices 1-3). For the molecular characterization of arthropods, the sequence comparison data of 18S and/or 28S rRNA gene are usually applied. Based on the 18S rRNA comparison result, SPA was not as closely related to MOBs/RDAs (98.7% identity; 23/1783 nucleotide mismatches), compared to MOBs and RDAs (99.8% identity; 2/1783 nucleotide mismatches). In addition, most mismatches (56.5%, 13/23) were located within a very short region (13/110 nts in length) close to the 5’ end of the 18S rRNA genes of SPA and MOBs/RDAs. Compared to 18S rRNA gene, distinct sequence diversity was noticed among the 28S rRNA genes of different mite species, suggesting that the 28S rRNA gene could be a better choice applied in species differentiation. The comparison of 28S rRNA nucleotide sequence alignments revealed that SPA was distinctly different from other mite species, but most similar to RDA and other mite in the family Myobiidae (Table 4B). Furthermore, phylogenetic differences (18S and 28S rRNA genes) among SPA and other different mites suggested that SPA was a novel member of *Myobia* genus

doi:10.6342/NTU202301649

in Myobiidae family (Fig 3). Besides 18S and 28S rRNA genes, the mitochondrial 16S rRNA gene has also been applied for mite classification (Sastre *et al.*, 2018). In this study, that the nucleotide sequence of a SPA fragment (~ 300 nts in length) was 100% identical to the mitochondrial 16S rRNA gene of *Myobia* sp. (KY649317; Sastre *et al.*, 2018) further supports SPA as a member of *Myobia* species. All above, both molecular and morphological characters indicate that this novel mouse fur mite Species A (SPA) is a new member of *Myobia* genus. Unfortunately, the relationship of SPA and MOB has not been confirmed in this study due to no MOB identified in Taiwan.

The rRNA secondary structures are highly conserved during evolution (Petrov *et al.*, 2014a; Ramesh *et al.*, 2016), providing additional phylogenetic information (Zhao *et al.*, 2013). In three-dimensional structures of rRNAs, the core of the rRNAs is common and conserved over the entire phylogenetic tree of living species (Petrov *et al.*, 2014a; Petrov *et al.*, 2015; Ramesh *et al.*, 2016). However, the surface regions of the rRNAs vary in primary, secondary, and tertiary structures (Petrov *et al.*, 2014a). Variations, such as expansions and deletions of a certain helix, in rRNA structure across species, provide specific taxonomy information in species identification (Zhao *et al.*, 2013; Petrov *et al.*, 2014a; Petrov *et al.*, 2014b; Petrov *et al.*, 2015). In this study, the predicted secondary structures, especially the 28S, are conserved in the common core and varied in length in distal branches. Our data show that in the remote region of the SPA 28S rRNA, several helices are observed to appear as expansion segments in the comparisons of the RDA and COP, indicating that the SPA is a distinct fur mite species to the RDA and COP.

Several challenges and difficulties have to overcome in order to characterize a tiny

doi:10.6342/NTU202301649

single mite in molecule biology and morphology simultaneously. In this study, after DNA extraction, the shell was collected and the species status of the specimens was determined. For molecular characterization of eukaryotes, ribosomal RNA genes (18S, 5.8S, and 28S) were commonly applied to construct the phylogeny. However, distinct sequence diversity of 5.8S and 28S rRNA and limited rRNA database of mites available, especially for members in Myobiidae family make it more challenging in primer design, rRNA amplification, and sequencing (Zhao *et al.*, 2013; Zhao *et al.*, 2020). Additionally, a limited amount of DNA and long length of 28S rRNA (about 4,500 bps) with complex secondary structures make it more difficult to obtain the whole sequences of one single mite (Zhao *et al.*, 2020). In this study, the 28S rDNA sequences of SPA and RDA-NTU were obtained through combining the sequences of several fragments of different individual mites and confirmed for more than one time. Attempts to obtain the sequences of 5.8S rDNA were not successful and only a short region of 28S rRNA of SPA was obtained. This may be due to the challenges of sequence diversity, limited database, RNA's fragility, and complex secondary structures. Attempts to complete 5.8S rDNA sequences are ongoing.

In summary, the molecular and morphological characteristics of a novel mouse fur mite, SPA, was determined. This is the first time to characterize a novel fur mite with molecule biology and morphology simultaneously. The phylogenetic data suggested that SPA was a novel mouse mite species in the family Myobiidae with MOB and RDA. Morphologically, SPA, externally indistinguishable from MOB, was suggested to be a novel member of *Myobia* genus. In addition, RDA-NTU and COP-NTU were molecularly and morphologically identical to previously published RDA and COP, respectively. In the future, it is important to develop a sensitive SPA-specific diagnosis assay for laboratory mouse health monitoring.

doi:10.6342/NTU202301649

References

1. **Council of Agriculture.** 2021. Animal Protection Act. ROC. https://law.moj.gov.tw/ENG/LawClass/LawAll.aspx?pcode=M0060027.
2. **Baker DG.** 1998. Natural pathogens of laboratory mice, rats, and rabbits and their effects on research. Clin Microbiol Rev. **11**:231-66. doi: 10.1128/CMR.11.2.231. PMID: 9564563. PMCID: PMC106832.
3. **Baker DG.** 2007. Parasites of rats and mice, p.359–368. In: Baker, DG, editor. Flynn's Parasites of Laboratory Animals, 2nd ed. Ames (IA): Blackwell Publishing.
4. **Ball-Goodrich LJ, Johnson E.** 1994. Molecular characterization of a newly recognized mouse parvovirus. J Virol. **68**:6476-6486. doi: 10.1128/JVI.68.10.6476-6486.1994. PMID: 8083985. PMCID: PMC237068.
5. **Bernier CR, Petrov AS, Waterbury CC, Jett J, Li F, Freil LE, Xiong X, Wang L, Migliozzi BLR, Hershkovits E, Xue Y, Hsiao C, Bowman JC, Harvey SC, Grover MA, Wartelle ZJ, Williams LD.** 2014. RiboVision suite for visualization and analysis of ribosomes. Faraday Discuss. **169**:195-207. DOI: 10.1039/c3fd00126a.
6. **Bochkov AV.** 2009. Mites of the family Myobiidae (Acari: Prostigmata) parasitizing rodents of the former USSR. Acarina. **17**:109-169.
7. **Bochkov AV.** 2010. A review of mammal-associated Psoroptidia (Acariformes: Astigmata). Acarina. **18**:99-260.
8. **Chen CH, Wang MH, Wan CH.** 2020. Multiplex polymerase chain reaction assay for the detection of five common endoparasite infestations in laboratory rodents. Taiwan Vet J. **46**:123-132. doi: 10.1142/S1682648520500110.
9. **Chou CL, Cheng YC, Wang MH, Wan CH.** 2020. Novel PCR assays for three

doi:10.6342/NTU202301649

fur mites in naturally infected mice without animal sacrifice. Taiwan Vet J. **46**:133-142. https://doi.org/10.1142/S1682648520500122.

10. **Council of Agriculture.** 2018. Guideline for the care and use of laboratory animals, Chinese-Taipei society of laboratory animal sciences, Taipei, ROC.
11. **Docampo R.** 2017. ZooBank registration requirement. J Eukaryot Microbiol. **64**:728. doi: 10.1111/jeu.12477. PMID: 29139237.
12. **Feldman SH, Ntenda AM.** 2011. Phylogenetic analysis of *Myobia musculi* (Schranck, 1781) by using the 18S small ribosomal subunit sequence. Comp Med. **61**:484-491. PMID: 22330574. PMCID: PMC3236689.
13. **Gerwin PM, Arbona RJR, Riedel ER, Henderson KS, Lipman NS.** 2017. PCR testing of IVC filter tops as a method for detecting murine pinworms and fur mites. J Am Assoc Lab Anim Sci. **56**:752-761. PMID: 29256370. PMCID: PMC5710154.
14. **Grove KA, Smith PC, Booth CJ, Compton SR.** 2012. Age-associated variability in susceptibility of Swiss Webster mice to MPV and other excluded murine pathogens. J Am Assoc Lab Anim Sci. **51**:789-796. PMID: 23294885; PMCID: PMC3508183.
15. **Hanson WH, Taylor K, Taylor DK.** 2021. PCR testing of media placed in soiled bedding as a method for mouse colony health surveillance. J Am Assoc Lab Anim Sci. **60**:306-310. doi: 10.30802/AALAS-JAALAS-20-000096. PMID: 33952384. PMCID: PMC8145126.
16. **Johnston NA, Trammell RA, Ball-Kell S, Verhulst S, Toth LA.** 2009. Assessment of immune activation in mice before and after eradication of mite infestation. J Am Assoc Lab Anim Sci. **48**:371-377. PMID: 19653944. PMCID: PMC2715926.
17. **Karlsson EM, Pearson LM, Kuzma KM, Burkholder TH.** 2014. Combined

doi:10.6342/NTU202301649

evaluation of commonly used techniques, including PCR, for diagnosis of mouse fur mites. J Am Assoc Lab Anim. Sci. **53**:69-73. PMID: 24411782. PMCID: PMC3894650.

18. **Klimov PB, OConnor BM, Chetverikov PE, Bolton SJ, Pepato AR, Mortazavi AL, Tolstikov AV, Bauchan GR, Ochoa R.** 2018. Comprehensive phylogeny of acariform mites (Acariformes) provides insights on the origin of the four-legged mites (Eriophyoidea), a long branch. Mol Phylogenet Evol. **119**:105-117. doi: 10.1016/j.ympev.2017.10.017. PMID: 29074461.
19. **Körner C, Miller M, Brielmeier M.** 2019. Detection of murine astrovirus and *Myocoptes musculinus* in individually ventilated caging systems: Investigations to expose suitable detection methods for routine hygienic monitoring. PLoS One. **14**:e0221118. doi: 10.1371/journal.pone.0221118. PMID: 31408494. PMCID: PMC6692027.
20. **Kumar S, Stecher G, Li M, Knyaz C, Tamura K.** 2018. MEGA X: molecular evolutionary genetics analysis across computing platforms. Mol Biol Evol. **35**:1547–1549. doi:10.1093/molbev/msy096.
21. **Lee MA, Shen Z, Holcombe HR, Ge Z, Franklin EG, Arbona RJR, Lipman NS, Fox JG, Sheh A.** 2019. Detection of *Myocoptes musculinus* in fur swab and fecal samples by using PCR analysis. J Am Assoc Lab Anim Sci. **58**:796-801. doi: 10.30802/AALAS-JAALAS-19-000046. PMID: 31662161; PMCID: PMC6926404.
22. **Liao JR, Ho CC, Ko CC.** 2021. Predatory mites (Acari: Mesostigmata: Phytoseiidae) intercepted from samples imported to Taiwan, with description of a new species. Zootaxa. **4927**:301-330. doi: 10.11646/zootaxa.4927.3.1. PMID: 33756698.

doi:10.6342/NTU202301649

23. **Lindstrom KE, Carbone LG, Kellar DE, Mayorga MS, Wilkerson JD.** 2011. Soiled bedding sentinels for the detection of fur mites in mice. J Am Assoc Lab Anim Sci. **50**:54-60. PMID: 21333164. PMCID: PMC3035404.

24. **Matsuda T, Fukumoto C, Hinomoto N, Gotoh T.** 2013. DNA-based identification of spider mites: Molecular evidence for cryptic species of the genus *Tetranychus* (Acari: Tetranychidae). J Econ Entomol. **106**:463–472. doi: 10.1603/EC12328.

25. **Morita E, Kaneko S, Hiragun T, Shindo H, Tanaka T, Furukawa T, Nobukiyo A, Yamamoto S.** 1999. Fur mites induce dermatitis associated with IgE hyperproduction in an inbred strain of mice, NC/Kuj. J Dermatol Sci. **19**:37-43. doi:10.1016/s0923-1811(98)00047-4.

26. **Morita T, Ohmi A, Kiwaki A, Ike K, Nagata K.** 2018. A new stubby species of demodectic mite (Acari: Demodicidae) from the domestic dog (Canidae). J Med Entomol. **55**:323-328. doi: 10.1093/jme/tjx226. PMID: 29309708.

27. **Mullen GR, OConnor BM.** 2019. Mites (Acari), p.533-602. In: Mullen GR, Durden LA, editors. Medical and Veterinary Entomology, 3rd ed. Academic Press. ISBN 9780128140437. doi: 10.1016/B978-0-12-814043-7.00026-1.

28. **National Research Council (US) Committee on Infectious Diseases of Mice and Rats.** 1991. Infectious diseases of mice and rats. National Academies Press (US). doi:10.17226/1429.

29. **Petrov AS, Bernier CR, Gulen B, Waterbury CC, Hershkovits E, Hsiao C, Harvey SC, Hud NV, Fox GE, Wartell RM, Williams LD.** 2014a. Secondary structures of rRNAs from all three domains of life. PLoS One. **9**:e88222. doi: 10.1371/journal.pone.0088222. PMID: 24505437. PMCID: PMC3914948.

30. **Petrov AS, Bernier CR, Hsiao C, Norris AM, Kovacs NA, Waterbury CC,**

doi:10.6342/NTU202301649

Stepanov, VG, Harvey SC, Fox GE, Wartell RM, Hud NV, Williams LD. 2014b. Evolution of the ribosome at atomic resolution. Proc Natl Acad Sci USA. **111**:10251-10256. doi: 10.1073/pnas.1407205111. PMID: 24982194. PMCID: PMC4104869.

31. **Petrov AS, Gulen B, Norris AM, Kovacs NA, Bernier CR, Lanier KA, Fox GE, Harvey SC, Wartell RM, Hud NV, Williams LD.** 2015. History of the ribosome and the origin of translation. Proc Natl Acad Sci USA. **112**:15396-15401. doi:10.1073/pnas.1509761112.
32. **Pochanke V, Hatak S, Hengartner H, Zinkernagel RM, McCoy KD.** 2006. Induction of IgE and allergic-type responses in fur mite-infested mice. Eur J Immunol. **36**:2434-2445. doi: 10.1002/eji.200635949. PMID: 16909433.
33. **Poppe SA.** 1896. Beitrag zur Kenntnis der Gattung Myobia v. Heyden. Zool Anz. **19**:327–333.
34. **Ramesh M, Woolford Jr JL.** 2016. Eukaryote-specific rRNA expansion segments function in ribosome biogenesis. RNA. **22**:1153-1162. doi: 10.1261/rna.056705.116. PMID: 27317789. PMCID: PMC4931108.
35. **Roediger B, Lee Q, Tikoo S, Cobbin JCA, Henderson JM, Jormakka M, O'Rourke MB, Padula MP, Pinello N, Henry M, Wynne M, Santagostino SF, Brayton CF, Rasmussen L, Lisowski L, Tay SS, Harris DC, Bertram JF, Dowling JP, Bertolino P, Lai JH, Wu W, Bachovchin WW, Wong, JJL., Gorrell MD, Shaban B, Holmes EC, Jolly CJ, Monette S, Weninger W.** 2018. An atypical parvovirus drives chronic tubulointerstitial nephropathy and kidney fibrosis. Cell. **175**:530-543.e24. doi: 10.1016/j.cell.2018.08.013. PMID: 30220458. PMCID: PMC6800251.
36. **Sastre N, Calvete O, Martínez-Vargas J, Medarde N, Casellas J, Altet L,**

doi:10.6342/NTU202301649

Sánchez A, Francino O, Ventura J. 2018. Skin mites in mice (*Mus musculus*): high prevalence of *Myobia* sp. (Acari, Arachnida) in Robertsonian mice. Parasitol Res. **117**:2139-2148. PUBMED:29728826. doi: 10.1007/s00436-018-5901-z.

37. **Schneider CA, Rasband WS, Eliceiri KW.** 2012. NIH Image to ImageJ: 25 years of image analysis. Nat Methods. **9**:671-675. doi: 10.1038/nmeth.2089. PMID: 22930834. PMCID: PMC5554542.
38. **Schrank PP.** 1781. Pediculus muris musculi. Enumeratio Insectorum Austriae Indigent. **1058**:513.
39. **Thigpen JE, Lebetkin EH, Dawes ML, Amyx HL, Caviness GF, Sawyer BA, Blackmore DE.** 1989. The use of dirty bedding for detection of murine pathogens in sentinel mice. Lab Anim Sci. **39**:324-327. PMID: 2548034.
40. **Trifinopoulos J, Nguyen LT, Haeseler A, Minh BQ.** 2016. W-IQ-TREE: a fast online phylogenetic tool for maximum likelihood analysis. Nucleic Acids Res. **44**:W232-W235. doi: 10.1093/nar/gkw256. PMID: 27084950. PMCID: PMC4987875.
41. **Wan CH, Söderlund-Venermo M, Pintel DJ, Riley LK.** 2002. Molecular characterization of three newly recognized rat parvoviruses. J Gen Virol. **83**:2075-2083. doi: 10.1099/0022-1317-83-8-2075. PMID: 12124471.
42. **Weiss EE, Evans KD, Griffey SM.** 2012. Comparison of a fur mite PCR assay and the tape test for initial and posttreatment diagnosis during a natural infection. J Am Assoc Lab Anim Sci. **51**:574-578. PMID: 23312085. PMCID: PMC3447445.
43. **Wobus CE, Karst SM, Thackray LB, Chang KO, Sosnovtsev SV, Belliot G, Krug A, Mackenzie JM, Green KY, Virgin IV HW.** 2004. Replication of Norovirus in cell culture reveals a tropism for dendritic cells and macrophages. PLoS Biol. **2**:e432. doi: 10.1371/journal.pbio.0020432. PMID: 15562321; PMCID:

doi:10.6342/NTU202301649

PMC532393.

44. **Zhao YE, Xu JR, Hu L, Wu LP, Wang ZH.** 2012. Complete sequence analysis of 18S rDNA based on genomic DNA extraction from individual *Demodex* mites (Acari: Demodicidae). Exp Parasitol. **131**:45-51. doi: 10.1016/j.exppara.2012.02.025. PMID: 22414329.

45. **Zhao YE, Wang ZH, Xu Y, Wu LP, Hu L.** 2013. Secondary structure prediction for complete rDNA sequences (18S, 5.8S, and 28S rDNA) of *Demodex folliculorum*, and comparison of divergent domains structures across Acari. Exp Parasitol. **135**:370-381. doi: 10.1016/j.exppara.2013.07.025. PMID: 23954189.

46. **Zhao Y, Zhang WY, Wang RL, Niu DL.** 2020. Divergent domains of 28S ribosomal RNA gene: DNA barcodes for molecular classification and identification of mites. Parasit Vectors. **13**:251. doi: 10.1186/s13071-020-04124-z. PMID: 32404192. PMCID: PMC7222323.

doi:10.6342/NTU202301649

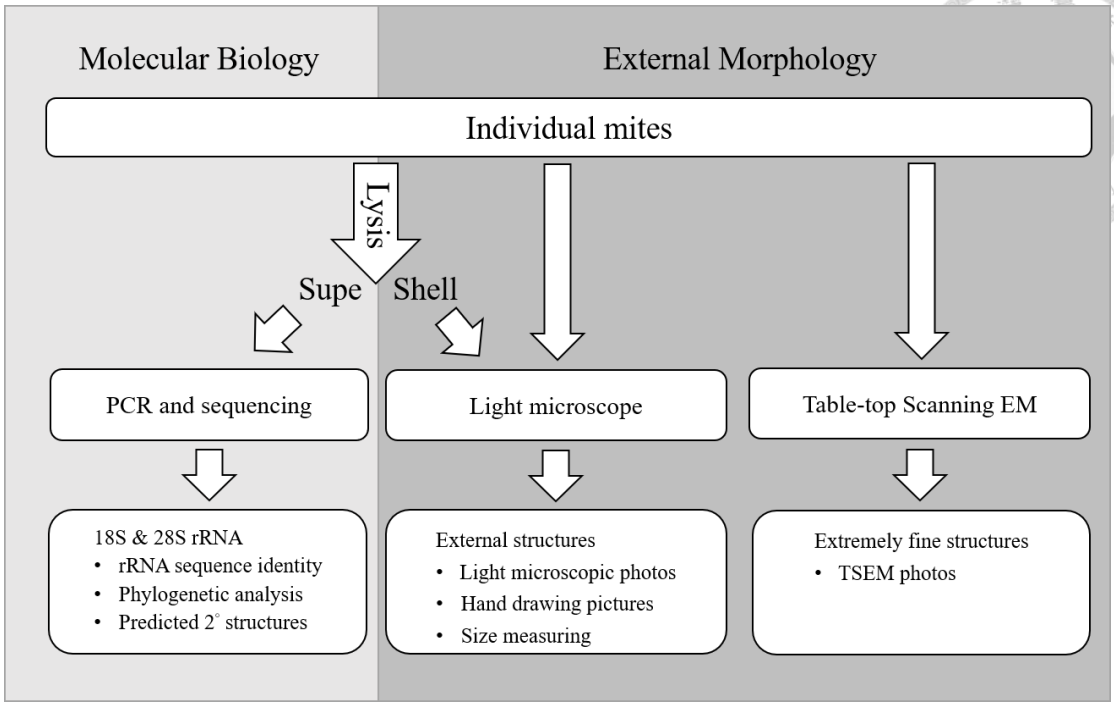

Fig 1. Experimental design

doi:10.6342/NTU202301649

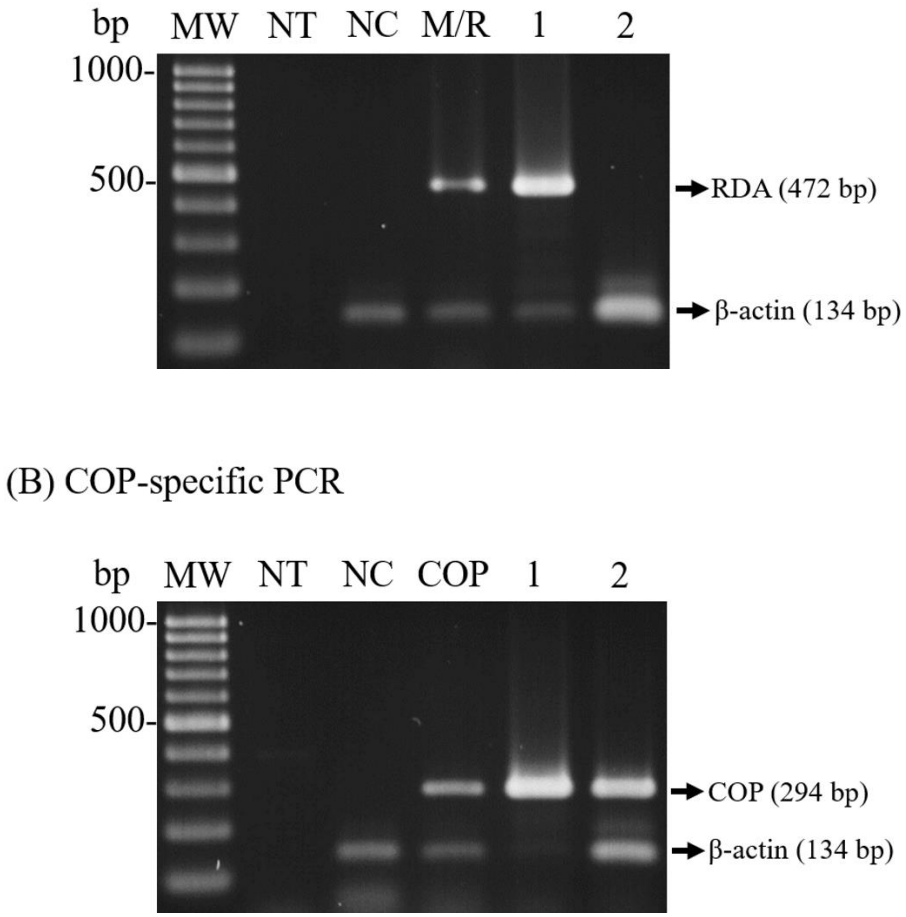

Fig 2. Detection of fur mites from clinical samples of Colony A and B by (A) the MOB/RDA-specific PCR assay and by (B) the COP-specific PCR assay.

MW: molecular weight marker; NT: no-template negative control; NC: no-parasite cage wipe control; M/R: RDA DNA mixed with no-parasite cage wipe sample; COP: COP DNA mixed with no-parasite cage wipe sample; Lane 1: the fur swab sample of mouse from Colony A; Lane 2: the fur swab sample of mouse from Colony B; RDA: *Radfordia affinis*; COP: *Myocoptes musculinus*.

doi:10.6342/NTU202301649

(A) 18S rRNA gene

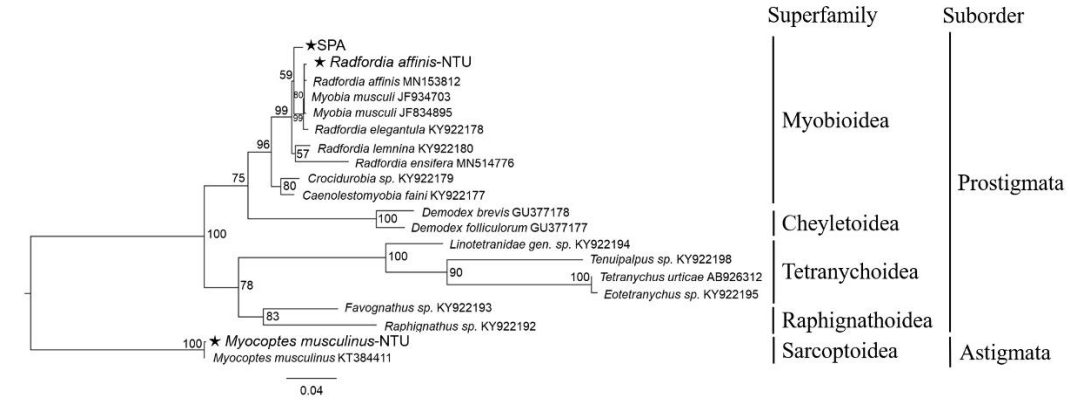

(B) 28S rRNA gene

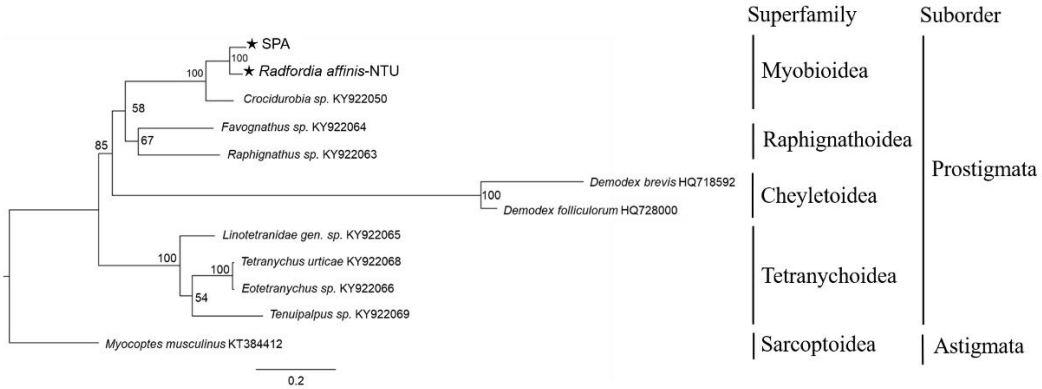

Fig 3. Phylogeny of (A) 18S rRNA gene and (B) 28S rRNA gene of mites on animals and plants. Phylogenetic analyses were performed using the neighbor-joining method based on Kimura's two-parameter model implemented in MEGA X. Numbers close to the nodes represent bootstrap values based on 1000 replicates. Bars, the number of substitutions per site.

★The mites identified in NTU, Taiwan.

SPA: Species A

doi:10.6342/NTU202301649

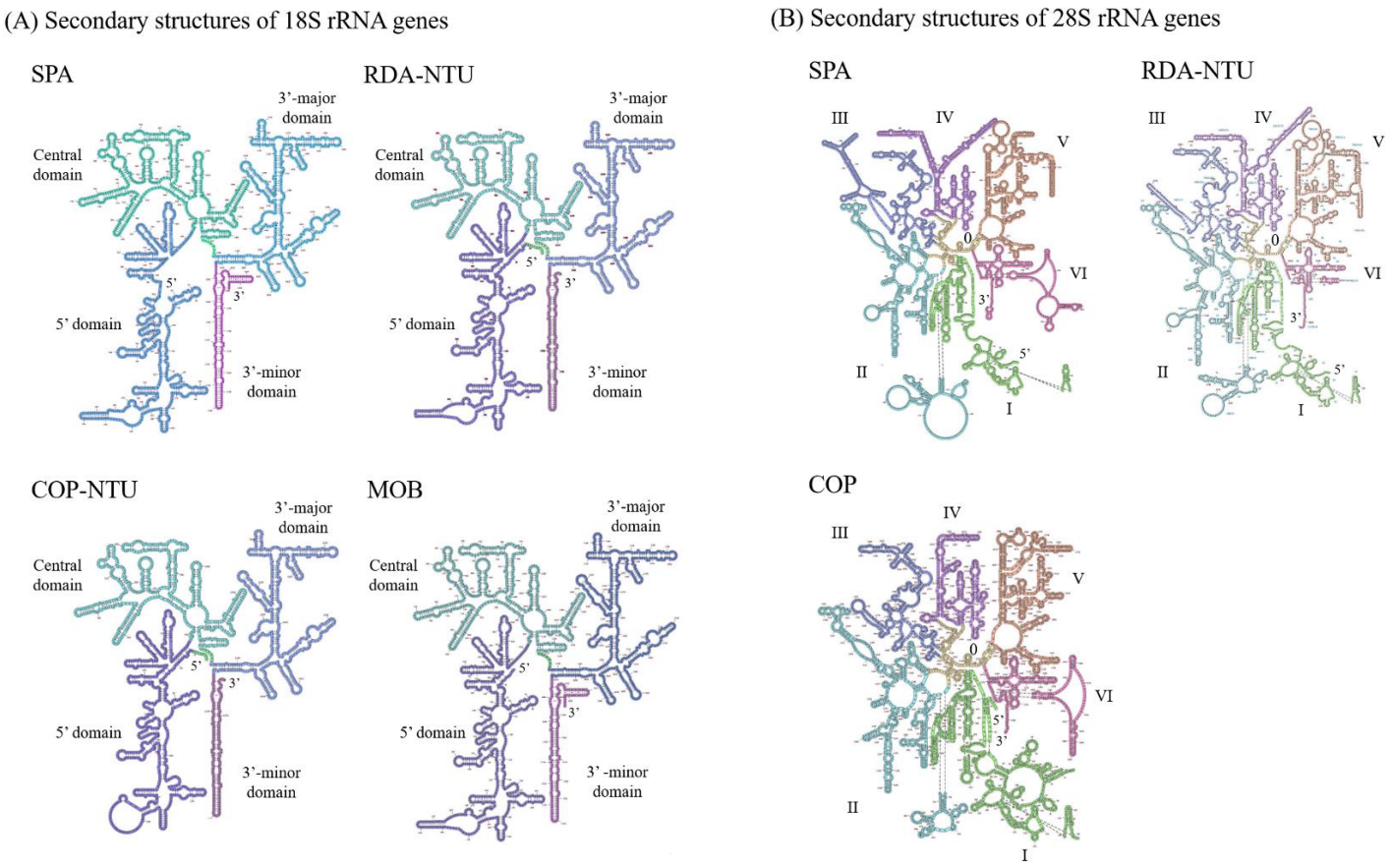

Fig 4. Predicted secondary structures of (A)18S rRNA gene and (B) 28S rRNA gene of fur mites. SPA: Species A; RDA-NTU: *Radfordia affinis*-NTU; COP-NTU: *Myocoptes musculinus*-NTU; MOB: *Myobia musculi*; COP: *Myocoptes musculinus*; four domains in 18S rRNA genes: 5', central, 3'-major, and 3'-minor; 6 domains in 28S rRNA genes: I-VI.

doi:10.6342/NTU202301649

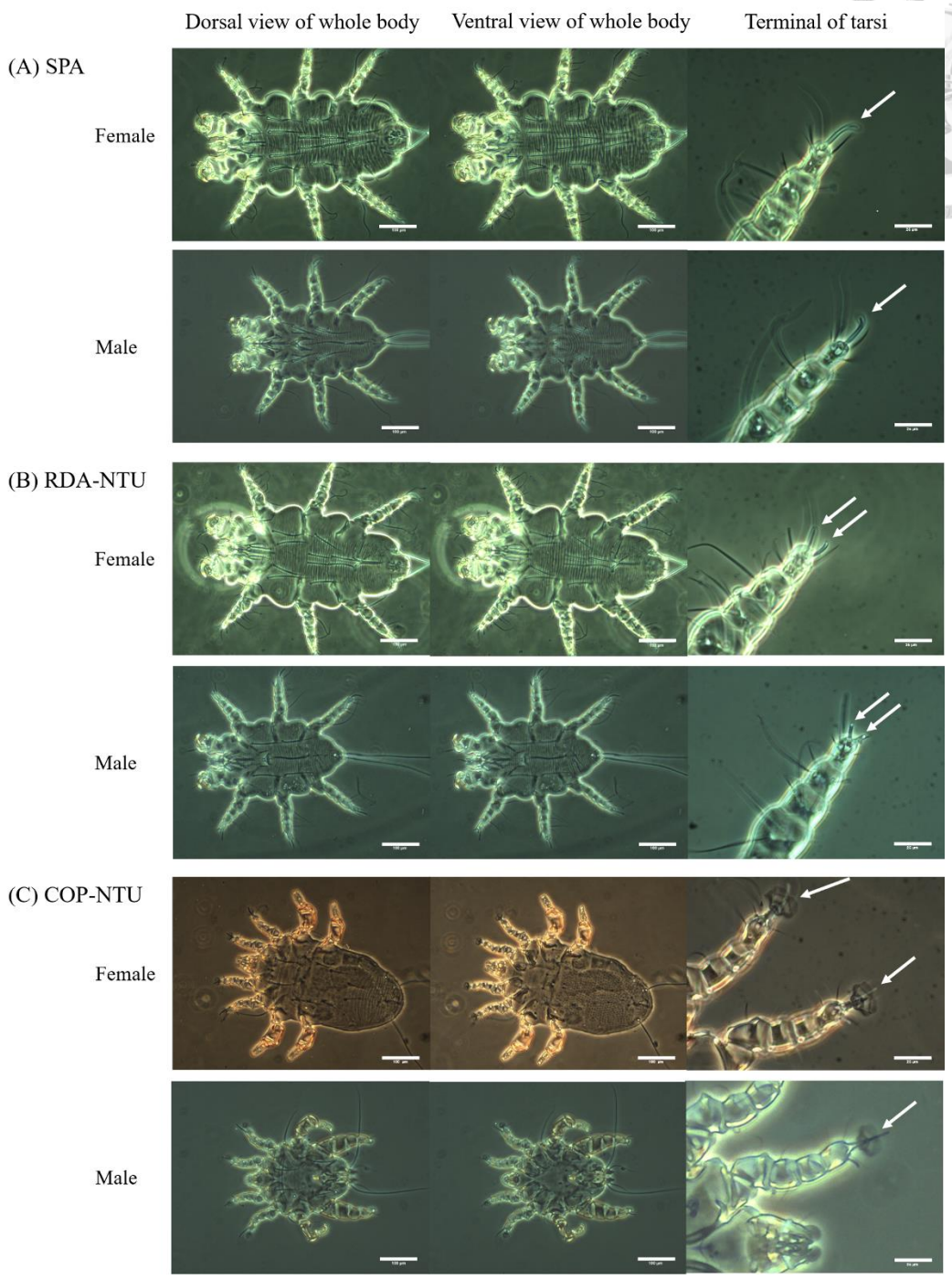

Fig 5. Adult morphology of the three fur mites. (A) SPA; (B) RDA-NTU; (C) COP-NTU. The arrows indicated the terminal structures of tarsi II (SPA and RDA-NTU) and tarsus I & II (COP-NTU). The view of whole body (magnification, 100×; bars, 100 μm); the view of terminal tarsi (magnification, 400×; bars, 25 μm).

SPA: Species A; RDA: *Radfordia affinis*; COP: *Myocoptes musculinus*.

doi:10.6342/NTU202301649

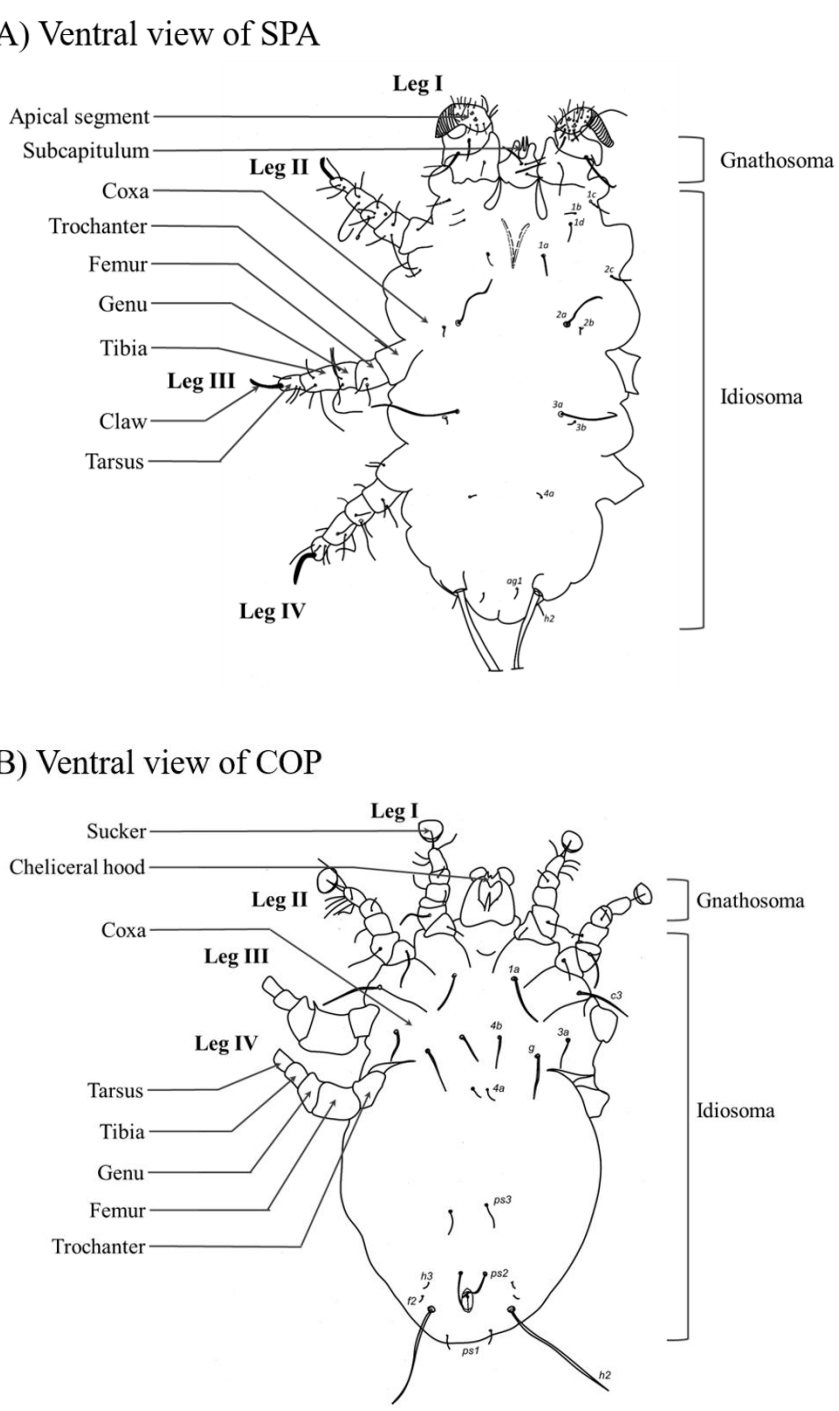

Fig 6. Morphology of fur mites. (A) Ventral view of SPA (B) Ventral view of COP.

SPA: Species A; COP: *Myocoptes musculinus*

doi:10.6342/NTU202301649

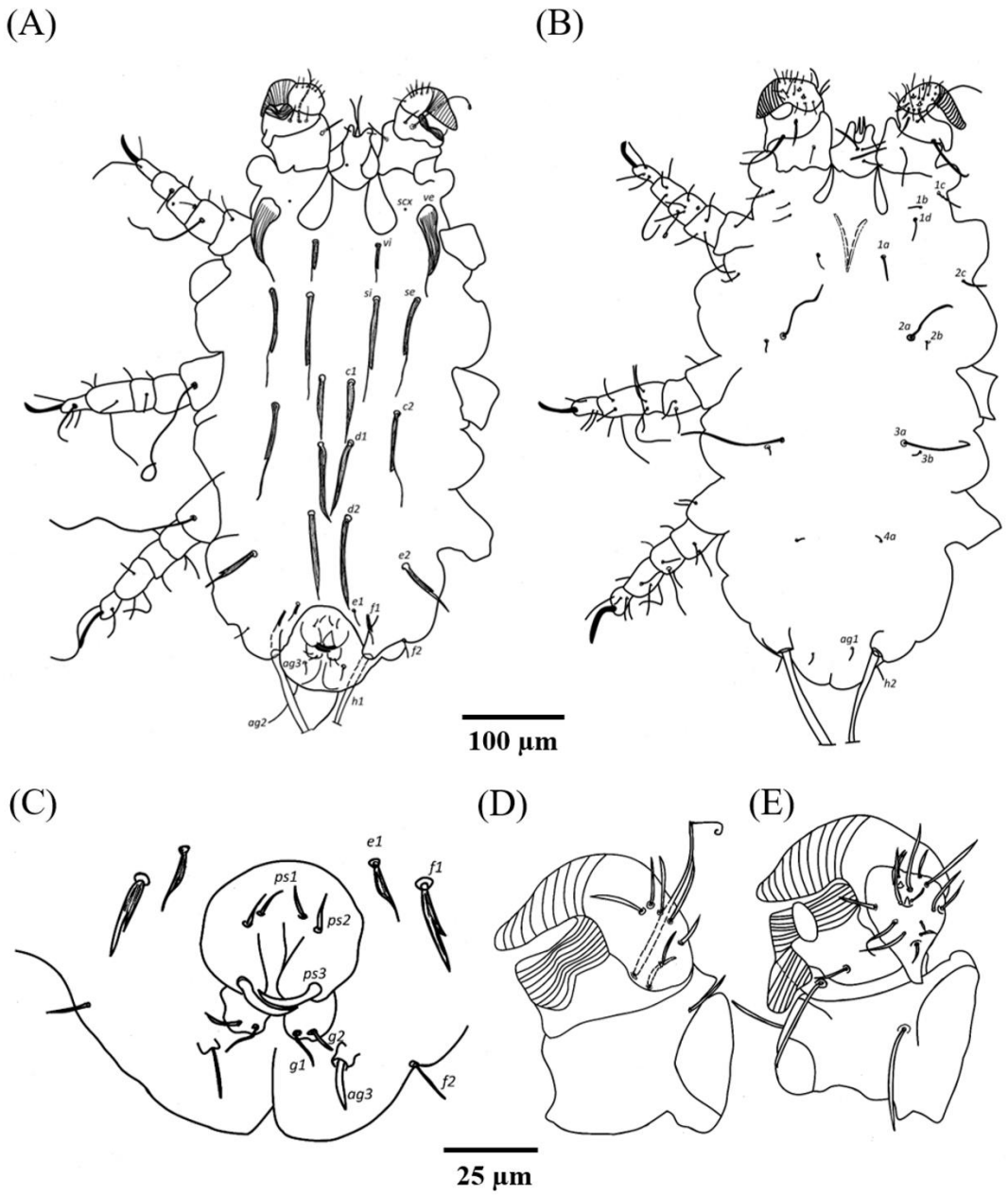

Fig 7. Drawing pictures of female SPA, species A, (A) dorsal view; (B) ventral view; (C) vulva; (D) dorsal view of tarsi I; (E) ventral view of tarsi I.

doi:10.6342/NTU202301649

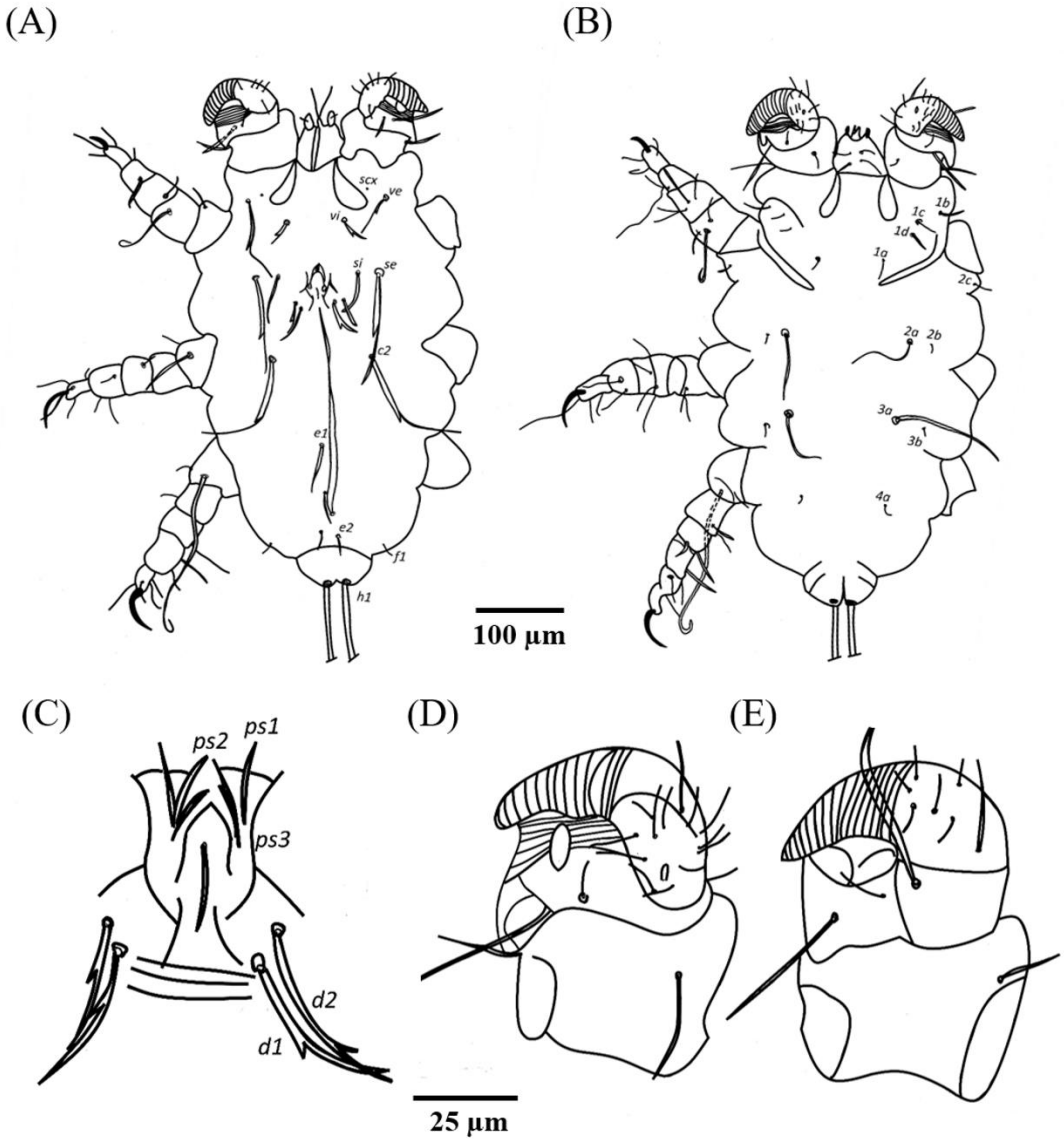

Fig 8. Drawing pictures of male SPA, species A, (A) dorsal view; (B) ventral view; (C) genital shield; (D) dorsal view of tarsi I; (E) ventral view of tarsi I.

doi:10.6342/NTU202301649

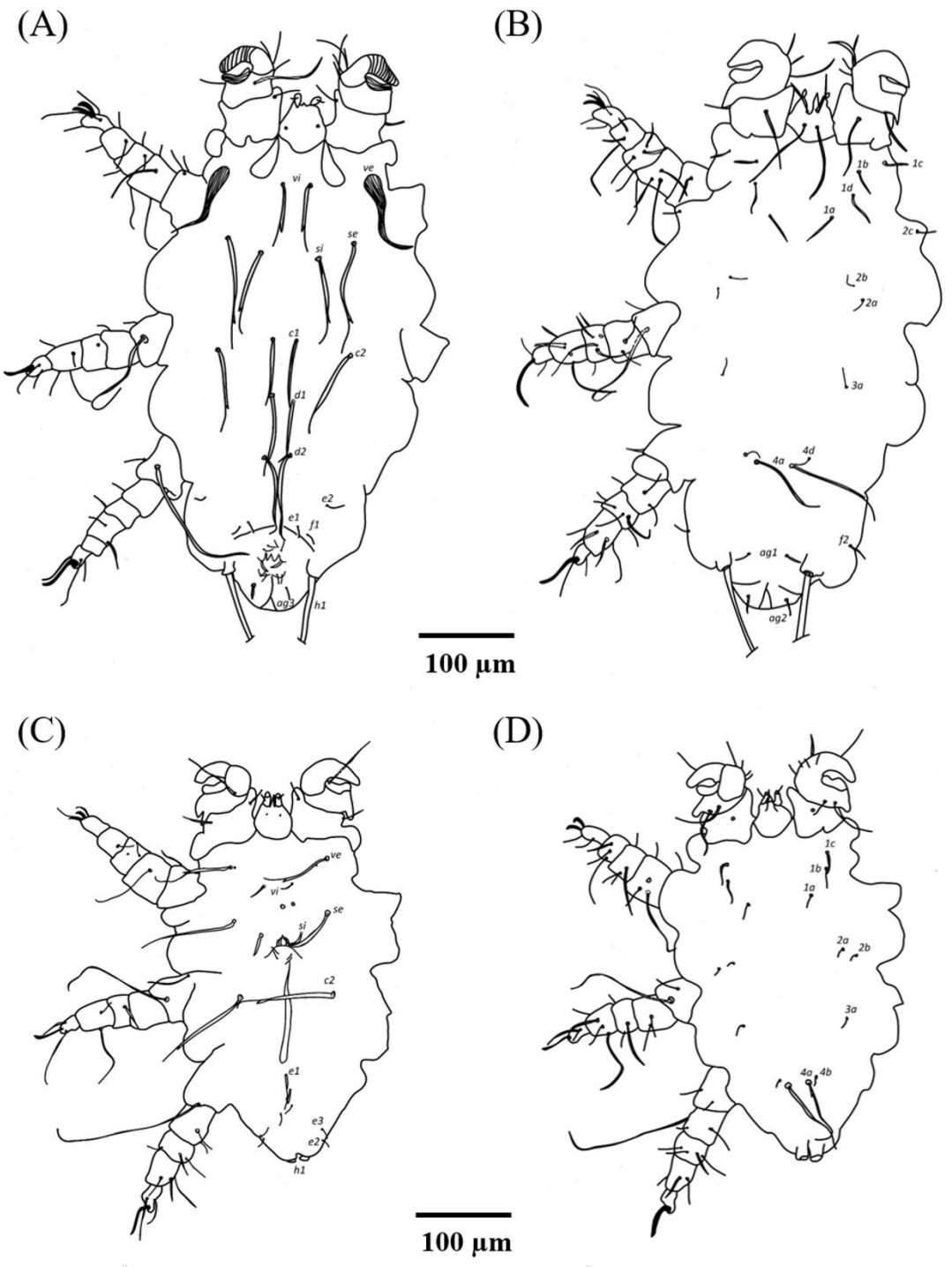

Fig 9. Drawing pictures of *Radfordia affinis* (Poppe, 1896), (A) female dorsal view; (B) female ventral view; (C) male dorsal view; (D) male ventral view.

doi:10.6342/NTU202301649

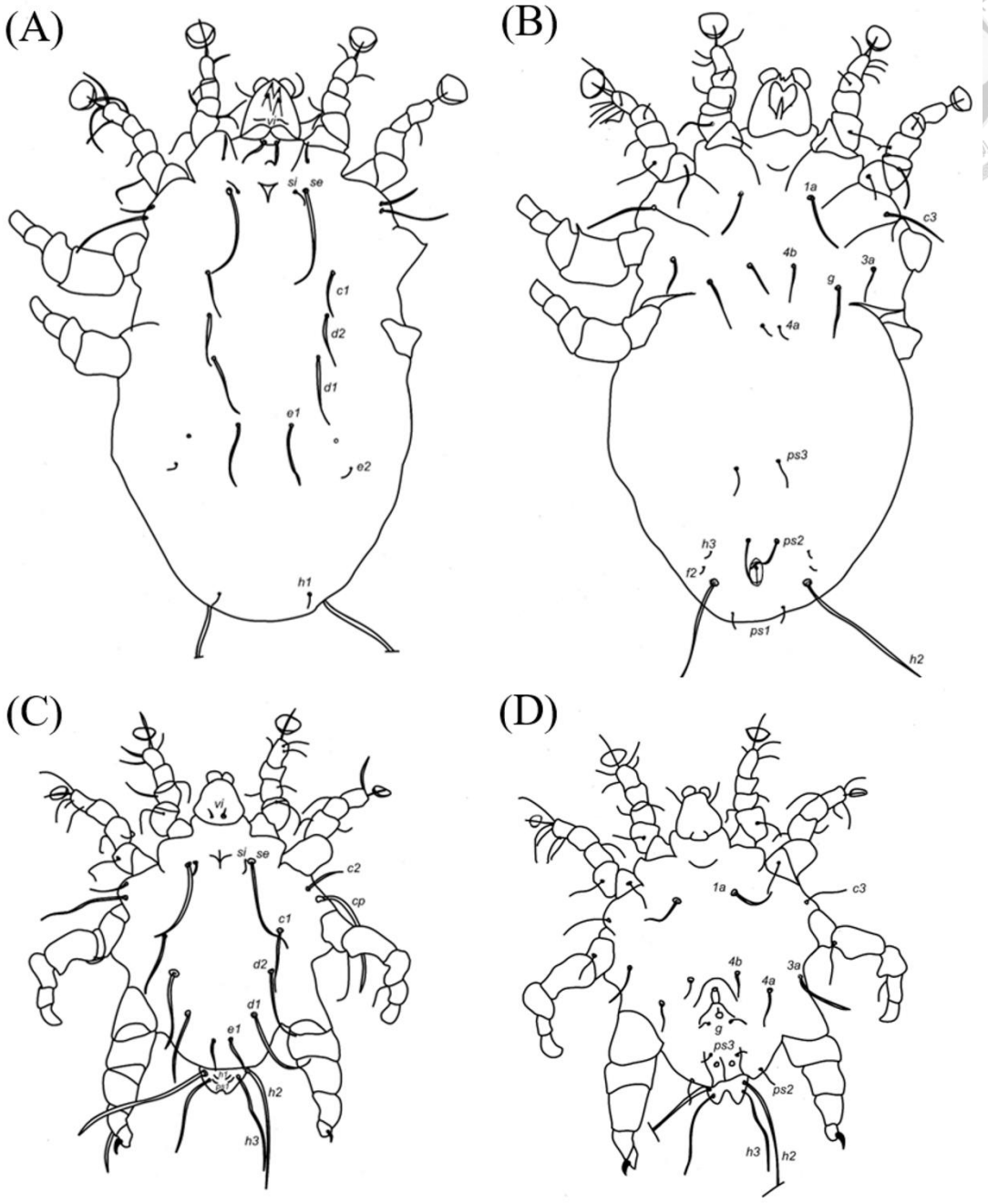

Fig 10. Drawing pictures of *Myocoptes musculinus* (Koch, 1840), (A) female dorsal view; (B) female ventral view; (C) male dorsal view; (D) male ventral view.

doi:10.6342/NTU202301649

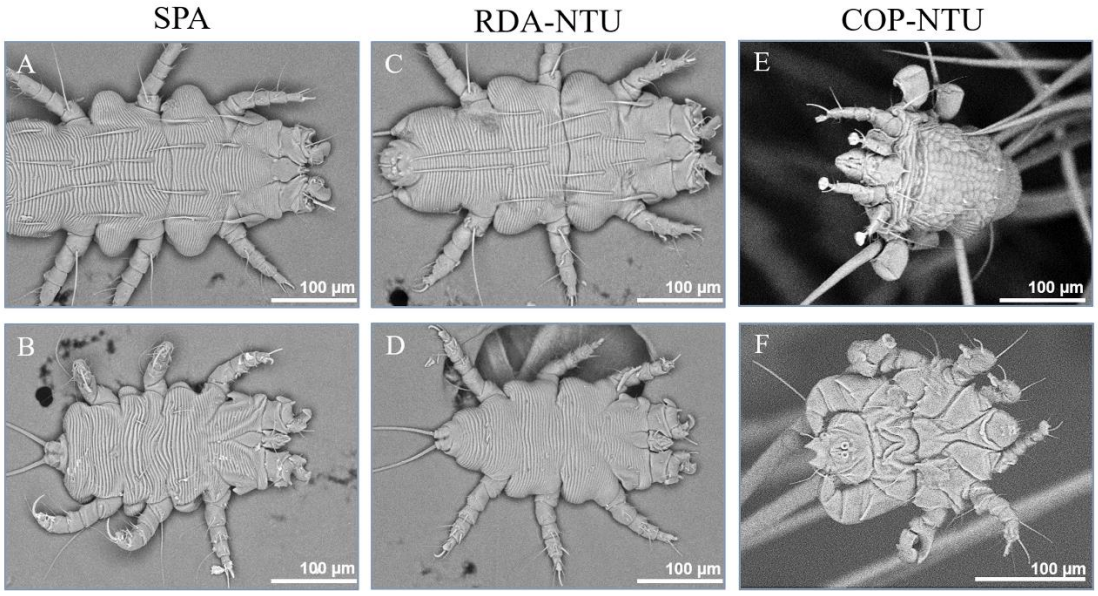

Fig 11. Morphology of fur mites under a tabletop scanning electron microscope (TSEM). (A) the dorsal view of female SPA (magnification: 400×; and bars: 100 μm); (B) the ventral view of male SPA (magnification: 400×; and bars: 100 μm); (C) the dorsal view of female RDA-NTU (magnification: 400×; and bars: 100 μm); (D) the ventral view of male RDA-NTU (magnification: 400×; and bars: 100 μm); (E) the dorsal view of female COP-NTU (magnification: 400×; and bars: 100 μm); (F) the ventral view of male COP-NTU (magnification: 500×; and bars: 100 μm).

SPA: Species A; RDA-NTU: *Radfordia affinis*-NTU; COP-NTU: *Myocoptes musculinus*-NTU

doi:10.6342/NTU202301649

Table 1. Information of laboratory mice, colony classification, and fur mite infestation (SPA, RDA, MOB, and COP) status in various mouse colonies.

	Stock/strains	Colony classification[1]	Animal No.	SPA[2]	COP[2]	RDA[2]	MOB[2]
Colony A (n=19)							
	ICR	C	9	9	9	9	0
	ICR-GEM	C	10	10	10	10	0
Colony B (n=13)							
	B6CBA -GEM	C	12	12	12	0	0
	B6.129S6-GEM	C	1	1	1	0	0
Total#			32	32	32	19	0

The infection status of each animal was determined by observation of adult fur mites and/or by PCR amplification, followed by DNA sequencing analyses.
[1]Colony Classification: C: conventional colony.
[2]SPA: Species A; RDA: *Radfordia affinis*; MOB: *Myobia musculi*; COP: *Myocoptes musculinus*

doi:10.6342/NTU202301649

Table 2. Information of numbers of three fur mites applied in various methods for molecular biology and morphology analyses.

Specise	Sex	Total#	Molecular biology		Morphology			
			PCR	Sequencing	Photo	Drawings	Measure	TSEM
SPA	Female	85	36	29	65	2	14	20
	Male	33	17	8	27	1	10	6
RDA	Female	49	26	10	45	1	12	4
	Male	14	3	2	10	1	4	4
COP	Female	49	11	7	20	1	3	29
	Male	28	1	0	13	1	3	15

doi:10.6342/NTU202301649

Table 3. The published mites used in phylogenetic analysis.

Species	Order	Suborder	Superfamily	Family	Accession numbers
Myobia musculi	Trombidiformes	Prostigmata	Myobioidea	Myobiidae	18S: JF934703 & JF834895
Radfordia affinis	Trombidiformes	Prostigmata	Myobioidea	Myobiidae	18S: MN153812
Radfordia ensifera	Trombidiformes	Prostigmata	Myobioidea	Myobiidae	18S: MN514776
Radfordia elegantula	Trombidiformes	Prostigmata	Myobioidea	Myobiidae	18S: KY922178
Radfordia lemnina	Trombidiformes	Prostigmata	Myobioidea	Myobiidae	18S: KY922180
Caenolestomyobia faini	Trombidiformes	Prostigmata	Myobioidea	Myobiidae	18S: KY922177
Crocidurobia sp.	Trombidiformes	Prostigmata	Myobioidea	Myobiidae	18S: KY922179; 28S: KY922050
Favognathus sp.	Trombidiformes	Prostigmata	Raphignathoidea	Cryptognathidae	18S: KY922193; 28S: KY922064
Raphignathus sp.	Trombidiformes	Prostigmata	Raphignathoidea	Raphignathidae	18S: KY922192; 28S: KY922063
Linotetranidae gen. sp.	Trombidiformes	Prostigmata	Tetranychoidea	Linotetranidae	18S: KY922194; 28S: KY922065
Tenuipalpus sp.	Trombidiformes	Prostigmata	Tetranychoidea	Tenuipalpidae	18S: KY922198; 28S: KY922069
Tetranychus urticae	Trombidiformes	Prostigmata	Tetranychoidea	Tetranychidae	18S: AB926312; 28S: KY922068
Eotetranychus sp.	Trombidiformes	Prostigmata	Tetranychoidea	Tetranychidae	18S: KY922195; 28S: KY922066
Demodex brevis	Trombidiformes	Prostigmata	Cheyletoidea	Demodicidae	18S: GU377178; 28S: HQ718592
Demodex folliculorum	Trombidiformes	Prostigmata	Cheyletoidea	Demodicidae	18S: GU377177; 28S: HQ728000
Myocoptes musculinus	Sarcoptiformes	Astigmata	Sarcoptoidea	Myocoptidae	18S: KT384411; 28S: KT384412

doi:10.6342/NTU202301649

Table 4(A). Percentage of the 18S rRNA nucleotide sequence identity among different mites using the clustal w method with default settings in MegAlign software (DNASTAR).

	RDA-NTU	MOB (Yale)	MOB (Virginia)	RDA	*Radfordia elegantula*	*Radfordia lemnina*	*Radfordia ensifera*	*Crocidurobia* sp.	*Caenolestomyobia faini*	*Favognathus* sp.	*Raphignathus* sp.	*Linotetranidae* gen. sp.	*Tenuipalpus* sp.	*Tetranychus urticae*	*Eotetranychus* sp.	*Demodex brevis*	*Demodex folliculorum*	COP	COP-NTU
SPA	98.7	98.8	98.8	98.8	98.6	98.4	96.1	96.9	97.2	90.9	89.6	90.2	88.7	88.0	88.0	90.8	91.5	86.5	86.5
RDA-NTU		99.6	99.8	99.7	99.5	98.2	96.4	96.6	96.8	90.3	89.1	89.8	88.3	87.7	87.7	90.6	91.3	86.2	86.3
MOB (Yale)			99.7	99.6	99.3	98.3	96.4	96.6	96.8	90.4	89.1	89.9	88.3	87.8	87.8	90.6	91.3	86.3	86.3
MOB (Virginia)				99.8	99.5	98.3	96.4	96.6	96.8	90.4	89.1	89.9	88.3	87.8	87.8	90.7	91.4	86.3	86.3
RDA					99.5	98.2	96.3	96.6	96.8	90.2	89.1	89.7	88.1	87.7	87.7	90.5	91.3	85.9	86.0
Radfordia elegantula						98.2	96.2	96.7	96.8	90.4	89.3	89.8	88.1	87.4	87.4	90.5	91.4	86.1	86.2
Radfordia lemnina							96.2	96.6	97.0	90.7	89.4	90.3	88.6	87.8	87.8	90.6	91.3	86.5	86.5
Radfordia ensifera								94.7	95.5	88.8	88.3	88.5	87.1	86.2	86.2	89.0	89.6	85.0	85.0
Crocidurobia sp.									98.3	91.2	89.9	90.9	88.7	88.1	88.1	90.9	91.6	86.5	86.6
Caenolestomyobia faini										91.2	89.6	90.7	88.7	88.1	88.1	90.9	91.6	86.5	86.6
Favognathus sp.											92.0	92.0	90.1	88.8	88.8	87.8	89.1	86.4	86.5
Raphignathus sp.												89.6	88.2	86.8	86.8	87.0	88.2	85.6	85.7
Linotetranidae gen. sp.													89.5	88.5	88.3	87.4	88.2	86.5	86.6
Tenuipalpus sp.														86.8	86.6	86.0	86.4	85.9	85.9
Tetranychus urticae															99.6	85.9	85.9	84.1	84.2
Eotetranychus sp.																85.9	85.9	84.1	84.2
Demodex brevis																	96.9	85.0	85.1
Demodex folliculorum																		85.3	85.3
COP																			99.9

doi:10.6342/NTU202301649

SPA: Species A; RDA-NTU: *Radfordia affinis*-NTU; MOB (Yale): *Myobia musculi* (JF834895); MOB (Virginia): *Myobia musculi* (JF934703); RDA: *Radfordia affinis* (MN153812); *Radfordia elegantula*: KY922178; *Radfordia lemnina*: KY922180; *Radfordia ensifera*: MN514776; *Crocidurobia* sp.: KY922179; *Caenolestomyobia faini*: KY922177; *Favognathus* sp.: KY922193; *Raphignathus* sp.: KY922192; *Linotetranidae* gen. sp.: KY922194; *Tenuipalpus* sp.: KY922198; *Tetranychus urticae*: AB926312; *Eotetranychus* sp.: KY922195; *Demodex brevis*: HQ718592; *Demodex folliculorum*: HQ728000; COP: *Myocoptes musculinus* (KT384411); COP-NTU: *Myocoptes musculinus*-NTU.

doi:10.6342/NTU202301649

Table 4(B). Percentage of the 28S rRNA nucleotide sequence identity among different mites using the Clustal W with default settings in MegAlign software (DNASTAR).

	RDA-NTU	*Crocidurobia* sp.	*Favognathus* sp.	*Raphignathus* sp.	*Linotetranidae* gen. sp.	*Tenuipalpus* sp.	*Tetranychus urticae*	*Eotetranychus* sp.	*Demodex brevis*	*Demodex folliculorum*	COP
SPA	93.7	87.8	78.7	78.0	74.6	72.5	76.0	76.0	71.4	75.0	74.7
RDA-NTU		89.4	78.4	77.7	74.8	73.7	76.1	76.1	71.2	74.2	74.7
Crocidurobia sp.			79.3	78.0	75.1	72.5	75.9	76.1	72.2	75.7	74.6
Favognathus sp.				81.0	79.1	77.8	79.2	79.3	74.0	75.8	75.8
Raphignathus sp.					77.2	75.6	77.7	77.7	72.9	75.2	74.8
Linotetranidae gen. sp.						83.9	86.5	86.4	73.2	72.9	76.6
Tenuipalpus sp.							83.7	83.7	72.3	72.0	75.8
Tetranychus urticae								99.5	73.0	74.2	75.2
Eotetranychus sp.									72.8	74.0	75.2
Demodex brevis										85.2	73.9
Demodex folliculorum											73.5

SPA: Species A; RDA-NTU: *Radfordia affinis*-NTU; *Crocidurobia* sp.: KY922050; *Favognathus* sp.: KY922064; *Raphignathus* sp.: KY922063; *Linotetranidae* gen. sp.: KY922065; *Tenuipalpus* sp.: KY922069; *Tetranychus urticae*: KY922068; *Eotetranychus* sp.: KY922066; *Demodex brevis*: HQ718592; *Demodex folliculorum*: HQ728000; COP: *Myocoptes musculinus* (KT384412).

doi:10.6342/NTU202301649

Appendix 1

Morphology of SPA

Family Myobiidae Mégnin

Genus *Myobia* van Heyden

Subgenus *Myobia* van Heyden

***Myobia* (*Myobia*) sp. (or *muris*)**

(Fig 7 & 8)

Diagnosis. Gnathosoma shorter than legs I. Subcapitulum with a pair of retrorse basal projections is on ventral view. Leg chaetotaxy of legs II–IV: coxae 3–2–1, trochanters 3–3–3, femora 5–3–3, genua 7+1 solenidion–5–5, tibiae 6–6–6, tarsi 7+1 solenidion–6–6. Coxal setae *1b*, *1c*, and *1d* not thickened. Dorsal seta of trochanters III–IV are whip-like. Apical segment of legs I is with ventral hook. Tarsi II-IV are with 1 claw each. Apical segment of legs I with ventral hook. Tarsi II–IV with 1 claw each.

Female (n=14). Body **559** 484 (315–559) long (gnathosoma included but legs I excluded), **222** 210 (167–278) wide. Body about 2x longer than wide. Dorsal idiosoma with a set of the idiosomal setae: propodonolal–internal vertical setae (*vi*), external vertical setae (*ve*), scapular external setae (*se*), scapular internal setae (*si*), dorsomedian–*c1, d1, e1, f1, h2,* dorsolateral–*c2, d2, e2, f2, h1,* intercoxal–*1a, 2a, 3a, 4a,* paragenital–*ag1-ag3,* genital–*g1, g2,*

doi:10.6342/NTU202301649

pseudoanal–*ps1-ps3*. Gnathosoma about **50** 46 (38-55) long. Setae *vi* **40** 40 (30–55) long, *c*. 5 wide, narrowly lanceolate, situated slightly anterior to *ve*; *ve* **90** 99 (83–110) long, *c*. 13 wide, narrowly lanceolate, almost reaching level of setal apices *si*; *se* **105** 97 (88–110) long, *c*. 8 wide, narrowly lanceolate, reaching level of setal apices *c*2; *si* **110** 104 (90–120) long, *c*. 5 wide narrowly lanceolate; *c1* **65** 71 (65–83) long, *d1* **78** 78 (65–93) long, and *d2* **90** 96 (85–110) long, all **5** 5 (4–5) wide, narrowly lanceolate, not overlapping, distances between bases *c1–d1* and *d1–d2* subequal, **75** 59 (38–80) long; *c2* **100** 91 (75–110) long, *c*. 5 wide, subequal or slightly longer than *se*; *e1* and *e2* very narrow lanceolate, **18** 21 (18–25) long and **65** 64 (55–73) long, respectively; *f1* **35** 25 (23–35) long, stick-like; *f2* and *h2* slightly thickened, stick-like, **15** 16 (10–25) long and **10** 12 (8–20) long, respectively; setal bases *e1* and *e2 s*ituated almost at same transverse level; all coxal setae filiform: *1a* **20** 20 (13–25) long, *2a*, *3a* **55** 71 (50–105) long and *4a* **20** 16 (10–20) long, respectively; *ag1* **13** 19 (13–25) long, slightly thickened in basal part; *ag2* and *ag3* **45** 43 (33–50) long and **15** 15 (10–20) long, respectively, stick-like, subequal to *c1*, *d1*, and *d2* and shorter than *si*. Opening of opisthosomal organ situated equidistantly from levels of setal bases *4a* and *ag1* (most anterior pair). Legs setae *d* of tibia II was **125** 105 (90–140) long, *d* of tibiae III and IV were **140** 148 (125–170) and **150** 173 (145–190) long, respectively. Claws of tarsi II–IV subequal.

Male (n=10). Body length **393** 346 (282–393) long (gnathosoma included but legs I excluded) and **185** 169 (148–185) wide. Set of the idiosomal setae: propodonolal–*vi*, *ve*, *se*, *si*,

doi:10.6342/NTU202301649

dorsomedian– *d2* and *e2*, dorsolateral–*c2, d1, e1, f1*, intercoxal–*1a–4a*, genital–*g1, g2*, pseudoanal–*ps1-ps3*. Body length about 2 times longer than wide. Gnathosoma about **35** 35 (30-43) long. Setae *vi* **23** 25 (20–35) long, *c*. 3 wide, narrowly lanceolate, situated slightly anterior to *ve*; *ve* **70** 73 (70–80) long, *c*. 4 wide, narrowly lanceolate, almost reaching level of setal apices *si*; *se* **100** 93 (80–105) long, *c*. 4 wide, narrowly lanceolate, reaching level of setal apices *c*2; *si* **38** 44 (38–50) long, *c*. 3 wide narrowly lanceolate; *d1* **30** 35 (25–45) long and *d2* **38** 36 (25–45) long, narrowly lanceolate, not overlapping, distances between bases *d1–d2* subequal, 5 long; *c2* **100** 103 (90–125) long, *c*. 5 wide, subequal or slightly longer than *se*; *e1* and *e*2 very narrow lanceolate, **38** 36 (30–48) long and **13** 12 (10–15) long, respectively, setal bases *e1* and *e2 s*ituated almost at same transverse level; *f1* **8** 11 (5–15) long, stick-like; all coxal setae filiform: *1a* **10** 13 (10–18) long, *2a*,and *3a* **80** 65 (35–100) long *4a* **15** 14 (10–15) long. Seta of *1b, 1c,1d, 2b, 2c*, and *3b* **13** 14 (10–20) long. Seta *d* of tibia II **65** 86 (65–100) long, *d* of tibiae III and IV **120** 115 (75–150) and **185** 165 (145–225) long, respectively. Claws of tarsi II–IV subequal.

Type specimen examined. Holotye: 1011-20C-10. Paratypes: 1015-19A-m1, 1028-19-1, 3, 4, 6, 7, 10, 11, 19, 1001-20A-4, 6, 8, 1001-20B-1, 1011-20A-2, 3, 17, 19, 20, 1011-20C-6, 10, 13, 1012-20-6, 8, 12 The laboratory animal facilities, Da' an Dist., Taipei City (25°01.0375' N, 121°32.3979' E, 5.3 m), total 24 specimens from 2 females and 5 males of *Mus musculus*. Nine specimens from 1 female and 2 male mice in facility 1: 1 specimen (female:

doi:10.6342/NTU202301649

no.1015-19A-m1) from 1 female ICR mouse in 20 Aug 2019 and 8 specimens (females: no.1011-20A-2, 3, 17, 19, 20 and 1011-20C-10, and males: no.1011-20C-6, 13) from 2 male ICR-GEM mice in 11 Mar 2020. Fifteen specimens form 1 female and 3 male mice in facility 2: 8 specimens (females: no.1028-19-1, 3, 4, 10, 11, and males: no.1028-19-6, 7, 19) from 1 male CBA/B6 mouse in 22 Oct 2019, 3 specimens (female: no.1012-20-6, and males: no.1012-20-8, 12) from 1 female CBA/B6 mouse in 12 Mar 2020, and 4 specimens (female: no.1001-20A-8, and males: no.1001-20A-4, 6, and 1001-20B-1) from 2 male CBA/B6 mice in 8 Jan 2020, Y. C. Cheng (NTU).

Remarks.

This new species, SPA, is similar to *Myobia musculi* based on the morphological description of Bochkov (2009). Although *M. musculi* is widely distributed worldwide and the most notorious fur mite in laboratories, we noticed that the present species have few morphological differences but distinct differences in molecular evidence. Further study would be focused on all fur mite species worldwide to investigate whether any cryptic species still exist.

doi:10.6342/NTU202301649

Appendix 2

Morphology of RDA-NTU

Genus *Radfordia* van Ewing

Subgenus *Radfordia* van Ewing

***Radfordia* (*Radfordia*) *affinis* van Poppe**

(Fig 9)

Diagnosis. Gnathosoma shorter than legs I. Subcapitulum with pair of retrorse basal projections on ventral view. Subcapitular setae *n* filiform. Setation of legs II–IV: coxae 3–1–2, trochanters 3–3–3, femora 5–3–3, genua 7+ 1 solenidion–6–5, tibiae 6–6–6, tarsi 7+1 solenidion–6–6. Coxal setae *1b, 1c*, and *1d* not thickened. Dorsal seta of trochanters III–IV whip-like (absent in species from Australian Muridae or short in species of subgroup praomys). Tarsi II with a pair of claws, tarsi III and IV with 1 claw each. Apical segment of legs I with ventral hook.

Female (n=12). Body length 485 (396–541) long (gnathosoma included but legs I excluded) and 215 (167–252) wide. Set of the idiosomal setae: propodonolal–*vi, ve, se, si*, dorsomedian–*c1, d1, e1, f1*, dorsolateral–*c2, d2, e2, f2, h1*, intercoxal–*1a–4a*, paragenital–*ag1-ag3*. Body length about 2 times longer than wide. Gnathosoma about 41 (35-48) long. Setae *vi* 65 (58–85) long, *c*. 4 wide, narrowly lanceolate, situated slightly anterior to *ve*; *ve* 90 (83–100) long, *c*. 7 wide, narrowly lanceolate, almost reaching level of

doi:10.6342/NTU202301649

setal apices *si*; *se* 117 (95–135) long, *c*. 5 wide, narrowly lanceolate, reaching level of setal apices *c2*; *si* 91 (75–100) long, *c*. 4 wide narrowly lanceolate; *c1* 71 (60–75) long, *d1* 85 (75–90) long, and *d2* 94 (75–120) long, all 5 (4–5) wide, narrowly lanceolate, not overlapping, distances between bases *c1–d1* and *d1–d2* subequal, 63 (40–75) long; *c2* 98 (85–115) long, *c*. 4 wide, subequal or slightly longer than *se*; *e1* and *e2* very narrow lanceolate, 11 (5–15) long and 13 (5–18) long, respectively; *f1* 11 (10–15) long, stick-like; *f2* slightly thickened, stick-like, 14 (8–25) long, respectively, setal bases *e1* and *e2* situated almost at same transverse level; all coxal setae filiform: *1a* 26 (20–30) long, *2a* and *3a* 17 (10–20) long and *4a* 94 (75–100) long, respectively; *ag1* 16 (13–20) long, slightly thickened in basal part; *ag2* and *ag3* 14 (10–20) long and 12 (5–18) long, respectively, they stick-like subequal to *c1*, *d1*, and *d2* and shorter than *si*. Seta of *1b, 1c,1d, 2b, 2c*, and *4b* 22 (10–30) long. Opening of opisthosomal organ situated equidistantly from levels of setal bases *4a* and *ag1* (most anterior pair). Setae *d* of tibia II 87 (60–105) long, d of tibiae III and IV 118 (85–140) and 187 (130–215) long, respectively. Claws of tarsi II–IV 2-1-1.

Male (n=4). Body length 326 (222–389) long (gnathosoma included but legs I excluded) and 170 (148–196) wide. Set of the idiosomal setae: propodonolal–*vi, ve, se, si*, dorsomedian–*e1*, dorsolateral–*c2, e2, e3, h1*, intercoxal–*1a, 2a, 3a, 4a*, pseudoanal–*ps1-ps3*. Body length about 2 times longer than wide. Gnathosoma about 42 (38-45) long. Setae *vi* 21 (20–25) long, *c*. 4 wide, narrowly lanceolate, situated slightly anterior to *ve*; *ve* 100 (85–110) long, *c*. 5 wide,

doi:10.6342/NTU202301649

narrowly lanceolate, almost reaching level of setal apices *si*; *se* 110 (105–120) long, *c*. 4 wide, narrowly lanceolate, reaching level of setal apices *c*2; *si* 33 (20–50) long, *c*. 4 wide narrowly lanceolate; *d1* 23 (20–25) long and *d2* 21 (20–25) long, narrowly lanceolate, not overlapping, distances between bases *d1–d2* subequal, 3 long; *c2* 100 (70–115) long, *c*. 4 wide, subequal or slightly longer than *se*; *e1, e2,* and *e3* very narrow lanceolate, 22 (20–25) long, 13 (10–15) long and 15 (10–20) long, respectively, setal bases *e1* and *e2 s*ituated almost at same transverse level; all coxal setae filiform: *1a* 21 (20–23) long, *2a*, and *3a* 9 (8–10) long, and *4a* 70 (63–75) long; f2 slightly thickened, stick-like, they 11 (10–15) long. Seta of *1b, 1c, 2b,* and *4b* 16 (8–23) long. Seta *d* of tibia II 78 (55–105) long, d of tibiae III and IV 101 (80–135) long and 166 (150–185) long, respectively. Claws of tarsi II–IV subequal.

Material examined. The laboratory animal facility, Da' an Dist., Taipei City (25°01.0375' N, 121°32.3979' E, 5.3 m), total 16 specimens from 4 males of *Mus musculus*. Four males in facility 1: 1 specimen (female: no.1034-19-1) from 1 male ICR mouse in 20 Nov 2019 and 15 specimens (females: no.1011-20A-1, 13, 15, 1011-20C-9, and 1011-20D-4, 6, 10, 12, 14, 35, 38, and males: no.1011-20D-5, 15, 16, 42) from 3 male ICR-GEM mice in 11 Mar 2020, Y. C. Cheng (NTU).

Remarks. RDA-NTU was identified as *Radfordia affinis* by morphological (Bochkov, 2009) and molecular characterization (MN153812).

doi:10.6342/NTU202301649

Appendix 3

Morphology of COP-NTU

Family Myocoptidae Gunther

Genus *Myocoptes* Claparede

***Myocoptes musculinus* van Koch,**

(Fig 10)

Diagnosis.

Cheliceral hood and ventral apophysis of movable digit present. Palpal segments fused dorsally. Idiosoma slightly elongate, dorso-ventrally flattened or subcylindrical (Trichoecius). Supracoxal sclerite distinct, supracoxal opening indistinct, setae *scx* absent. Genital papillae present. Intercoxal attaching organs absent. Legs III and IV in females and immature stages and legs III in males modified into clasping organs. Femora of these legs enlarged and ventrally concave, genua distinctly developed; tibia and tarsi devoid of the pretarsi and shortened. Clasping apparatus formed by all these podomeres, excluding trochanters. Tarsi-genual part curving inward and fixings host hair between femoral concavity and these 3 podomeres. Ambulacral sclerites small but recognizable.

Female (n=3). Body length (gnathosoma included but legs I excluded) 496 (448–544) long and 256 (233–278) wide. Opisthogastral shields absent. Ovipore Y-shaped. Epigynum absent. Anal opening situated terminally or ventrally. Oviparous. Dorsal striated idiosomal cuticle

doi:10.6342/NTU202301649

without scales. Posterior median projection of propodonotal shield triangular about 5. Setae *se* about 6 times longer than *si*. Scales posterior to hysteronotal shield present. Striated cuticle posterior to oviporus densely covered by triangular scales. Setal bases *ps2* situated distinctly anterior to level of setal bases *f2*. Distance *ps2–ps2* not more than 2 times longer than *ps3–ps3*. Lengths of setae: *vi* 16 (12–22), *si* 19 (16–22), *se* 110 (97–125), *c1* 40 (31–53), *c2* 41 (38–44), *c3* 43 (34–56), *cp* 99 (94–109), *d1* 59 (44–72), *d2* 44 (38–52), *e1* 73 (53–91), *e2* 15 (13–16), *f2* 9 (9–10), *h1* 12 (12–13), *h2* 233 (200–250), *h3* 16, *1a* 49 (47–53), *3a* 37 (25–47), *4a* 16, *4b* 35 (31–38), *g* 37 (28–47), *ps1* 25 (16–31), *ps2* 30 (19–38), *ps3* 18 (15–20).

Male (n=3). Body length (gnathosoma included but legs I excluded) 328 (316–338) long and 218 (188–238) wide. Opisthosomal lobes and paranal suckers present. Legs III and IV normally developed. Legs IV of male without ambulacra. Striated idiosomal cuticle without scales. Setae *se* long longer than *si* about 6 times. All coxal fields without scales and lobes. Adanal suckers small, not more than 4. Lengths of setae: *vi* 6, *si* 18 (15–22), *se* 108 (93–122), *c1* 54 (43–69), *c2* 38 (31–41), *c3* 46 (28–66), *cp* 120 (113–125), *d1* 68 (59–78), *d2* 63 (44–79), *e1* 31 (28–34), *h1* 9, *h2* 254 (231–266), *h3* 69 (66–72), *1a* 39 (34–44), *3a* 37 (31–44), *4a* 32 (19–44), *4b* 25 (19–28), *g* 11 (10–13), *ps1* 9, *ps2* 32 (28–38), and *ps3* 7 (6–9).

Material examined. The laboratory animal facilities, Da' an Dist., Taipei City (25°01.0375' N, 121°32.3979' E, 5.3 m), *Mus musculus*: 3 males. Three specimens (females: no.1001-20A-12, 13, 1001-20B-12) from 2 male CBA/B6 mice in facility 2 in 8 Jan 2020, 3

doi:10.6342/NTU202301649

specimens (males: no.1004-21-1, 3, 7) from 1 male ICR-GEM mouse in facility 1 in 6 Jul 2021., Y. C. Cheng (NTU).

Remarks. COP-NTU was identified to *Myocoptes musculinus* by morphological (Bochkov, 2010) and molecular (KT384411) characterization.

doi:10.6342/NTU202301649